Available online at www.sciencedirect.com
ScienceDirect
Geochimica et Cosmochimica Acta 70 (2006) 5957–5989
Geochimica
www.elsevier.com/locate/gca

Evolved mare basalt magmatism, high Mg/Fe feldspathic crust, chondritic impactors, and the petrogenesis of Antarctic lunar breccia meteorites Meteorite Hills 01210 and Pecora Escarpment 02007

James M.D. Day [a,*], Christine Floss [b], Lawrence A. Taylor [a], Mahesh Anand [a,c,1], Allan D. Patchen [a]

[a] *Planetary Geosciences Institute, Department of Earth and Planetary Sciences, University of Tennessee, Knoxville, TN 37996, USA*
[b] *Laboratory for Space Sciences, Washington University, St. Louis, MO 63130, USA*
[c] *Department of Mineralogy, The Natural History Museum, Cromwell Road, London SW7 5BD, UK*

Received 1 December 2005; accepted in revised form 1 May 2006

Abstract

Antarctic lunar meteorites Meteorite Hills 01210 and Pecora Escarpment 02007 are breccias that come from different regolith lithologies on the Moon. MET 01210 is composed predominantly of fractionated low-Ti basaltic material and is classified as an immature, predominantly basaltic glassy matrix regolith breccia. PCA 02007 is a predominantly feldspathic regolith breccia consisting of metamorphosed feldspathic, noritic, troctolitic and noritic-anorthosite clasts, agglutinate and impact-glasses, as well as a number of basaltic clasts with mare and possible non-mare affinities. The basalt clasts in MET 01210 have undergone 'Fenner' trend enrichments in iron and may also have witnessed late-stage crystallization of zircon or a zirconium-rich mineral. Some of the features of MET 01210 are similar to other basaltic lunar breccia meteorites (e.g., Northwest Africa 773; Elephant Moraine 87521/96008; Yamato 793274/981031), but it is not paired with them. The presence of metamorphic anorthositic clasts as well as agglutinates indicates a small regolith component. Similarities with previously discovered evolved (e.g., LaPaz Icefield 02205; Northwest Africa 032) and ferroan (e.g., Asuka 881757; Yamato 793169) basaltic lunar meteorites suggest a similar mare source region for MET 01210. Despite lack of evidence for pairing, PCA 02007 shares many features with other feldspathic regolith breccias (e.g., Yamato 791197, Queen Alexandra Range 94281), including a high Mg/Fe whole-rock composition, glass spherules, agglutinate fragments and a diverse clast inventory spanning the range of ferroan anorthosite and high magnesium suite rocks. Some of the basalt fragments in this sample are fractionated and have an igneous origin. However, the majority of the basalt fragments are impact melt clasts. PCA 02007 supports previous studies of feldspathic lunar meteorites that have suggested an aluminous crust for the Moon, with compositions more similar to magnesium granulite breccias than ferroan anorthosites. A 'chondrule-like' fragment found in PCA 02007 and unlike any previously described lunar material is described and tentatively identified as the remnants of a chondritic lunar impactor. This clast is porphyritic with equant olivines that have forsterite-rich cores ($Fo_{>98}$), extreme normal zonation to more fayalitic rims ($Fo_{>44}$), and a mineral assemblage with rare earth element abundances distinct from described lunar material and more similar to chondrules found in ordinary or carbonaceous chondrites. Its discovery and description is significant for understanding the composition of lunar impactors. Previously, the main evidence for chondritic lunar impactors was from chondritic relative abundances and near chondritic ratios of highly siderophile elements in lunar impact melt breccias. However, the presence of this clast, along with two other chondritic clasts from Apollo soils 12037 and 15602, provides clues to the identity of ancient meteorite impactors on the Moon.

* Corresponding author. Fax: +1 865 974 2368.
E-mail address: jday13@utk.edu (J.M.D. Day).
[1] Present address: Centre for Earth, Planetary, Space and Astronomical Research, Department of Earth Sciences, The Open University, Milton Keynes, UK.

0016-7037/$ - see front matter © 2006 Elsevier Inc. All rights reserved.
doi:10.1016/j.gca.2006.05.001

1. Introduction

Brecciated lunar meteorites represent complex amalgamations of mineral fragments, lithic clasts and matrix

material that have been assembled through impact processes on the Moon. Such meteorites are well-lithified mixtures of near-surface material that are likely to represent average mineralogies and chemistries of their lunar source regions (Warren, 2003). Significant detailed research has been done on lunar breccia meteorites (e.g., Delaney, 1989; Warren and Kallemeyn, 1989; Hill et al., 1991; Anand et al., 2003; Gnos et al., 2004), and the data obtained from these feldspathic and basaltic materials has been compared with lunar remote sensing data, as well as regolith cores and hand-specimens collected during the Apollo and Luna missions.

Studies of lunar regolith breccia meteorites have provided new, and sometimes controversial, insights into the geochemical evolution of the Moon. Chief amongst these are: (1) important age constraints on events in lunar history (e.g., Borg et al., 2004; Gnos et al., 2004); (2) the likelihood that samples collected during the Apollo missions are only representative of the geochemically anomalous Procellarum KREEP Terrane (PKT) of the Moon, and not of the lunar surface as a whole (Warren, 2003; Korotev, 2005); (3) the apparent preponderance of low-titanium and very-low titanium mare basalt compositions in lunar meteorites relative to the quantity of high-Ti mare basalt returned from Apollo missions (Warren and Kallemeyn, 1989; Jolliff et al., 1998; Warren, 2003); (4) the lack of a temporal or chemical dichotomy between 'nonmare' and 'mare' volcanism on the Moon (e.g., Warren and Kallemeyn, 1989, 1991); (5) improved estimates of crustal aluminium contents and the possible magnesium-rich nature of the lunar highlands relative to estimates from ferroan anorthosites collected during the Apollo missions (Korotev et al., 2003) and; (6) confirmation that anorthositic and noritic anorthosite highland rocks are some of the most abundant lithologies on the lunar surface (e.g., Jolliff et al., 1991; Koeberl et al., 1996).

In this study, we examine two lunar breccia meteorites, Meteorite Hills (MET) 01210 and Pecora Escarpment (PCA) 02007, discovered in Antarctic in 2001 and 2003, respectively. Initial classification of MET 01210 considered it a lunar feldspathic regolith breccia, while PCA 02007 was considered a predominantly basaltic lunar breccia meteorite (McCoy and Welzenbach, 2003, 2004). Preliminary characterization studies have recognized that, in fact, the opposite is true, and MET 01210 is predominantly basaltic (Arai et al., 2005; Huber and Warren, 2005; Patchen et al., 2005; Zeigler et al., 2005a) whereas PCA 02007 is a feldspathic regolith breccia (Taylor et al., 2004a; Zeigler et al., 2004)! In an effort to elucidate the petrogenesis of these breccias and their components we have performed detailed petrological and geochemical studies of the breccias and of specific clasts within them.

Studies of Apollo and Luna breccia clasts (e.g., Coish and Taylor, 1978; Hunter and Taylor, 1983; Taylor et al., 1983; Dickinson et al., 1985; Norman et al., 1991; Norman and Taylor, 1992) have enabled the identification of a range of rock-types not recognized in the large, single-lithology grab samples of the Apollo missions. Such studies have also extended the age range of basaltic magmatism on the Moon (e.g., Taylor et al., 1983) and the age of the oldest lunar rocks, the ferroan anorthosite suite (e.g., Carlson and Lugmair, 1988; Alibert et al., 1994). Our efforts focus on two basaltic clasts in MET 01210 and an included 'chondrule-like' fragment in PCA 02007, providing new information on evolved mare basaltic magmatism, the nature of the highlands crust, and the description of a unique silicate meteorite occurring within the lunar regolith.

2. Analytical methods

Polished thin sections of PCA 02007 and MET 01210 (surface areas range from 50 to 100 mm^2) were obtained from the Meteorite Working Group for petrographic and mineralogical examination. Mineral modes were determined on polished sections with the *Feature Scan Phase Distribution* software package of an Oxford instrument energy dispersive spectrometer interfaced to the CAMECA SX-50 electron microprobe analyzer (EMPA), at the University of Tennessee. Modal analysis acquisition was performed using an accelerating potential of 15 keV, a 4 nA beam current and 70 mS count times sampling every 8 μm. Data bin parameters for this method are provided in Table 1.

Electron microprobe analyses were performed on two polished sections of PCA 02007 and one polished section of MET 01210. Mineral compositions were determined in wavelength dispersive spectral mode on the EMPA using an accelerating potential of 15 keV, a 20 nA beam current (30 nA for metals), 1 μm beam size, peak and background counting times of 20–30 s and standard ZAF (PAP) correction procedures. Glass and plagioclase compositions were determined using a 10 nA beam current, a 5–10 μm beam size and longer counting times to avoid mobilization of Na. A combination of natural and synthetic standards were used for calibration and were measured periodically within analytical sessions to ensure data quality. Drift was within counting error throughout every analytical session. Detection limits (3σ above background) are <0.03 wt% for SiO_2, TiO_2, Al_2O_3, MgO, CaO, Na_2O, K_2O and Cl, <0.05 wt% for Cr_2O_3, MnO, FeO, P_2O_5, NiO and Co, and <0.05–0.1 wt% for all other oxides and elements listed.

Concentrations of trace elements, including rare earth elements (REE), were determined using the modified Cameca ims 3f ion microprobe at Washington University, according to techniques described by Zinner and Crozaz (1986a). All analyses were made using an O^- primary beam and energy filtering at low mass resolution to remove complex molecular interferences. The resulting mass spectrum is deconvolved in the mass ranges K–Ca–Sc–Ti, Rb–Sr–Y–Zr and Ba-REE to remove simple molecular interferences that are not eliminated with energy filtering (Alexander, 1994; Hsu, 1995). Sensitivity factors for the REE are from Zinner and Crozaz (1986b) and those for other elements are from Hsu (1995) and are listed in Table 1 of Floss

Table 1
Modal analysis (as area and inferred volume percent) of clasts in MET 01210 and PCA 02007

MET 01210										PCA 02007 Chondrule Clast	
Clast ID	A[a]	AA[a]	AA	BB	H	K	L	M	N	T8[a]	T8
Plagioclase	35.6	75.1	67.4	—	8.9	17.7	85.1	89.0	72.2	19.9	[48.0]
Pyroxene	—	—	21.6	66.4	77.1	68.3	14.9	10.5	27.8	—	—
Clinopyroxene	36.8	12.4	—	—	—	—	—	—	—	—	—
Pigeonite	16.1	1.0	—	—	—	—	—	—	—	—	—
Fe-pyroxene	6.4	3.8	—	—	—	—	—	—	—	—	—
Olivine	—	—	11.0	—	—	14.0	—	—	—	46.2	44.8
Forsterite	<0.1	1.3	—	—	—	—	—	—	—	—	—
Fayalite	0.2	4.9	—	—	—	—	—	—	—	—	—
Oxides	—	—	—	15.1	14.0	—	—	—	—	<0.1	—
Ilmenite	0.3	<0.1	—	—	—	—	—	—	—	—	—
Ulvospinel	3.4	<0.1	—	—	—	—	—	—	—	—	—
Chromite	<0.1	<0.1	—	—	—	—	—	—	—	—	—
Phosphate	0.2	0.1	—	—	—	—	—	—	—	—	—
Silica	0.6	0.3	—	14.7	—	—	—	—	—	—	—
K-feldspar	0.1	0.1	—	—	—	—	—	—	—	—	—
Glass	—	—	—	3.8	—	—	—	—	—	28.8	[48.0]
FeS	0.3	0.9	—	—	—	—	—	—	—	4.7	[7.2]
FeNi metal	—	—	—	—	—	—	—	0.5	—	0.2	[7.2]
Total	100	100	100	100	100	100	100	100	100	100	100
	Basalt	Fd-Bas		Ev-Bas	Ev-Bas	Pic-Bas	Anorth	Anorth	Anorth	Chon	Chon

PCA 02007

Clast ID	T38	T35	T28	T9	T7	E	Y	ZD	F	T2	T1	U	V	W	X
Plagioclase	62.1	37.5	51.8	74.1	58.1	82.4	60.6	83.2	51.9	90.3	81.5	45.9	74.6	85.2	61.8
Pyroxene	35.1	62.5	25.0	—	33.5	7.1	—	—	34.2	4.2	—	54.1	25.4	14.8	31.2
Augite	—	—	—	—	—	—	26.5	—	—	—	—	—	—	—	—
Opx	—	—	—	—	—	—	12.9	16.8	—	—	—	—	—	—	—
Olivine	0.2	—	23.2	25.9	5.8	6.7	—	—	13.9	3.8	18.5	—	—	—	7.0
Oxides and FeNi metal	2.6	—	—	—	2.6	3.8	—	—	—	1.8	—	—	—	—	—
Total	100	100	100	100	100	100	100	100	100	100	100	100	100	100	100
	Fd-Bas	Bas	Gabbro	Troc	Bas	Gab-An	Norite	Norite	Gabbro	Anorth	Troc	Gabbro	Norite	Gab-An	Bas

Abbreviations: Fd-Bas = Feldspar-rich 'basalt,' Bas = Basalt, Ev-Bas = Evolved basalt, Pic-Bas = Picro basalt, Anorth = Anorthosite, Chon = 'Chondrule,' Troc = Troctolite, Gab-An = Gabbro anorthosite. Modal analysis for the majority of clasts was performed using back-scattered electron images. Thresholds for individual minerals were calculated according to analyzed mineral compositions and then quantitatively analyzed using NIH image analysis (freeware) software. Mineral modes using this method compare well with those measured using the *Feature Scan* method (see clast AA and clast T8 for comparisons). Reproducibility of this NIH image analysis technique is ~5%.

[a] Modal analysis using *Feature Scan Phase Distribution* software. Data bins for MET 01210 defined according to—Plagioclase = 35–55% Si, 11–40% Ca, 20–46% Al; Pigeonite = 46–72% Si, 4–12% Ca, 2–46% Mg, 0–4% Al; Clinopyroxene = 0–5% Al, 42–72% Si, 11–41.5% Ca, 2–42% Mg; Fe-pyroxene = 42–70% Si, 0–2% Mg, 7–32% Ca, 0–5% Al, 11–50% Fe; Ilmenite = 47–76% Ti, 18–45% Fe; Fayalite = 30–55% Si, 0-3% Ca, 35–62% Fe; Olivine = 10–45% Mg, 30–53% Si; Ulvöspinel = 20–49% Ti, 0–28% Cr; Cr-Spinel = 20–74% Cr, 0–20% Ti; Phosphate = 15–80% P, 19–69% Ca; K-feldspar = 50–100% Si, 10–30% Al, 6–25% K; FeS = 20–100% Fe, 25–100% S; Silica = 85–100% Si. See Taylor et al. (1996) for further information on the *Feature Scan Phase Distribution* technique.

et al. (1998). Absolute concentrations were determined using sensitivity factors relative to Si for silicates and Ca for phosphates, with SiO_2 and CaO concentrations determined by EMPA of the specific grains chosen for ion probe analysis. Reported errors are 1σ and are due to counting statistics only.

A 0.535 g powdered sub-sample of PCA 02007 (13) was provided by the Meteorite Working Group for whole-rock geochemical studies. Major element concentrations were measured on a 50 mg aliquot using an Optima 3300 Inductively Coupled Plasma Optical Emission Spectrometer (ICP-OES) at the University of Notre Dame following the procedures of Shafer et al. (2004). Whole-rock trace element measurements were also obtained on a 50 mg aliquot by solution mass spectrometry using a PlasmaQuad PQII STE machine following the procedure of Neal (2001). Because no powdered subsample of MET 01210 was available for study, 25 analyses of the fusion crust of the polished section were measured using the EMPA. Although fusion crust data may not faithfully record the whole-rock composition of the meteorite, averages of fusion crust major element compositions may be used as a proxy, especially for small meteorite samples (Day et al., 2006).

3. Results

The most widely utilized method for characterizing mineralogical and textural variations in brecciated materials is to break down the components according to lithological types. The descriptions made here for MET 01210 and PCA 02007 are representative, but not exhaustive, and focus on the most abundant and best preserved clast types. A summary of mineral modes, clast sizes and mineral compositions for both meteorites can be found in Tables 1–8.

3.1. Petrography and mineral chemistry of MET 01210

MET 01210 is a 22.8 g lunar breccia, discovered in the Meteorite Hills region of Antarctica in 2001 and was found partially covered (~30% of surface area) in a dark, highly vesiculated fusion crust. Using the terminology of Stöffler et al. (1980), the meteorite can be considered to be an

Table 2
Compositional ranges of representative lithic clasts in MET 01210 and PCA 02007

Clast	Dimensions (mm)	Textures/features	Pyroxene	Plagioclase	Olivine	Mineralogy
MET 01210 Immature Predominantly Basaltic Glassy Matrix Regolith Breccia						
Basaltic clasts						
A	3.0 × 2.5	Allotriomorphic granular	$Wo_{21}En_{49}$–Wo_1En_3	An_{97-80}	Fo_{7-3}	Ulv, Ilm, Mer, FeS, Sil
AA	0.7 × 0.5	Subophitic	$Wo_{17}En_{20}$–$Wo_{42}En_{3.5}$	$An_{94\pm2}$	Fo_{41-6}	FeS
BB	0.4 × 0.3	Skeletal Ilm/Granular	$Wo_{22}En_{20}$–$Wo_{23}En_1$	—	—	Ilm, Ba-Gl, Sil, FeS
H	0.3 × 0.2	Skeletal Ilm/Granular	$Wo_{28}En_{17}$–$Wo_{14}En_{0.5}$	$An_{88.6\pm1.1}$	—	Ulv, Ilm
K	0.8 × 0.6	Plumose	$Wo_{23}En_{45}$–$Wo_{24}En_3$	$An_{91\pm1}$	Fo_5	—
Anorthositic clasts						
M	0.5 × 0.4	Granular	$Wo_{38}En_{50}$–$Wo_{73}En_{23.5}$	$An_{96.6\pm0.6}$	—	FeNi metal
N	0.8 × 0.6	Granular	$Wo_{22}En_{21}$	$An_{97.0\pm0.7}$	—	FeNi metal
T	0.2 × 0.2	Granular	$Wo_{18}En_{53}$	$An_{96.1}$	—	FeNi metal
PCA 02007 Feldspathic Regolith Breccia						
Basaltic clasts						
T38	0.08 × 0.05	Subophitic	$Wo_{10}En_{55}$	$An_{96.9\pm0.6}$	Fo_{55}	Ilm
U	0.13 × 0.13	Granular	$Wo_{15}En_{45}$–$Wo_{27}En_{31}$	An_{96-90}	—	—
Impact melt Basaltic clasts						
E	0.4 × 0.2	Poikilitic	Wo_9En_{62}–$Wo_{15.5}En_{59}$	$An_{96.6\pm1.3}$	$Fo_{63.7\pm0.1}$	—
X	0.12 × 0.12	Poikilitic	Wo_3En_{60}–$Wo_{44}En_{42}$	$An_{94\pm1}$	Fo_{68-52}	Ilm
T35	0.15 × 0.10	Pilotaxitic/subophitic	Wo_5En_{73}–$Wo_{19}En_2$	An_{95-87}	—	FeS
T7	0.10 × 0.10	Pilotaxitic/subophitic	Wo_4En_{71}–Wo_9En_{67}	$An_{89\pm1}$	$Fo_{70.2\pm0.6}$	FeS, Phos
Troctolite clasts						
T9	0.2 × 0.1	Poikilitic	—	$An_{95.9\pm0.4}$	$Fo_{64.6\pm0.1}$	—
Tl	0.15 × 0.12	Poikilitic	—	$An_{96.0\pm0.7}$	$Fo_{79.0\pm0.1}$	—
Gabbro, Norite and Anorthosite clasts						
V	0.15 × 0.15	Subophitic	$Wo_{2.5}En_{67}$–$Wo_{40}En_{45}$	$An_{97.8\pm0.6}$	—	—
T28	0.3 × 0.3	Ophitic	$Wo_{20}En_{55}$	An_{97}	Fo_{60}	—
F	0.45 × 0.45	Ophitic	$Wo_{12}En_{62}$–$Wo_{35}En_{44}$	$An_{97.7\pm0.5}$	$Fo_{65.6\pm0.5}$	—
Y	0.25 × 0.15	Ophitic	$Wo_{2.5}En_{59}$–$Wo_{27}En_{41}$	$An_{96.2\pm1.0}$	—	—
ZD	0.07 × 0.07	Poikilitic	$Wo_{2.4}En_{82}$–Wo_3En_{74}	$An_{96.6\pm0.3}$	—	—
T2	0.3 × 0.2	Poikilitic	Wo_4En_{67}–$Wo_{39}En_{45}$	$An_{95.8\pm0.7}$	$Fo_{63.7\pm0.5}$	FeNi metal
W	0.15 × 0.10	Poikilitic	$Wo_{35}En_{44}$	$An_{92.5\pm1.0}$	$FO_{86.2\pm0.2}$	—

Average clast size for MET 01210 is around 0.6 × 0.6 mm versus 0.20 × 0.16 mm for PCA 02007. Mineralogy abbreviations are ulvöspinel (Ulv), ilmenite (Ilm), merrillite (Mer), troilite (FeS), silica (Sil), K–Ba-rich glass (Ba–Gl), iron–nickel metal grains (FeNi metal), unidentified (uncertain stoichiometry) phosphate (Phos).

Table 3
Representative EMPA data for silicate, oxide, phosphate and accessory phases in MET 01210

Phases Sample	Pyroxene Clast A	Pyroxene Clast A	Pyroxene Clast K	Pyroxene Clast M	Pyroxene Min Clast	Fe-Px Clast A	Fe-Px Min Clast	Olivine Clast A	Olivine Min Clast	Fayalite Clast A	Fayalite Min Clast	Plag Clast A	Plag Clast M	Plag Min Clast
wt%														
SiO_2	51.8	49.8	47.3	54.3	51.2	46.3	45.4	33.7	42.0	29.9	29.5	45.4	44.0	52.2
TiO_2	0.54	0.88	2.01	0.64	0.53	0.46	0.61	0.05	<0.03	0.11	0.12	—	—	—
Al_2O_3	1.36	1.15	5.63	1.08	1.29	0.31	0.52	<0.03	0.16	<0.03	<0.03	34.0	34.7	29.0
Cr_2O_3	0.55	0.24	0.73	0.36	0.37	<0.05	<0.05	0.13	0.15	<0.05	<0.05	—	—	—
FeO	18.8	25.1	20.5	15.3	24.0	44.3	45.9	46.9	5.45	66.3	68.6	0.36	0.30	0.82
MnO	0.37	0.45	0.33	0.28	0.42	0.83	0.56	0.53	0.06	0.85	0.81	—	—	—
MgO	16.7	12.7	10.6	26.6	17.6	1.60	0.19	18.2	52.9	1.94	0.37	0.22	0.10	0.03
CaO	9.94	9.33	13.4	1.74	4.70	5.75	6.30	0.38	0.33	0.82	0.75	19.2	19.6	13.6
Na_2O	<0.03	0.06	0.03	<0.03	<0.03	<0.03	<0.03	—	—	—	—	0.68	0.44	3.09
K_2O	—	—	—	—	—	—	—	—	—	—	—	<0.03	<0.03	0.63
Total	100.1	99.8	100.5	100.4	100.0	99.5	99.5	100.0	101.1	100.0	100.1	99.8	99.1	99.3
Mg#	61.3	47.4	48.0	75.6	56.8	6.0	0.8	41.0	94.5	5.0	1.0	An = 93.9	An = 96.1	An = 68.2

Phases Sample	Spinel Clast A	Spinel Min Clast	Ilm Clast H	Ilm Min Clast	Glass Clast BB	Glass Agg O	Glass Agg O_p[a]	Glass Matrix	Glass Matrix	Merri Clast A	Apatite Matrix		FeNi Clast M	FeNi Matrix
wt%														
SiO_2	0.03	0.08	0.03	0.04	58.0	48.4	46.0	44.7	44.3	0.29	1.46	Fe	93.8	90.4
TiO_2	31.4	7.60	51.7	52.4	—	1.76	0.42	0.19	1.38	—	—	Co	0.31	1.72
ZrO_2	—	—	0.05	0.23	—	—	—	—	—	—	—	Ni	5.51	7.45
Al_2O_3	1.82	11.5	0.09	0.10	20.3	17.6	19.1	30.5	17.2	—	—	S	0.04	<0.05
V_2O_3	—	0.59	—	—	—	—	—	—	—	—	—	P	0.65	<0.05
Cr_2O_3	3.61	38.8	<0.05	0.07	—	0.41	0.47	<0.05	0.28	—	—	Si	0.04	0.06
FeO	62.0	39.7	47.2	46.7	0.53	11.6	12.5	3.48	13.4	5.07	1.95	Cr	<0.05	<0.05
MnO	0.26	0.29	0.36	0.38	—	0.23	0.19	0.07	0.19	—	—	Ti	0.04	0.04
MgO	0.30	1.20	<0.03	01.20	<0.03	5.38	8.34	3.23	7.15	0.64	0.03	Ca	0.32	0.37
CaO	<0.03	<0.03	0.09	0.12	0.77	13.4	12.6	17.6	15.0	38.2	52.5			
P_2O_5	—	—	—	—	—	0.18	0.19	0.04	0.22	40.9	39.4	Total	100.7	100.1
BaO	—	—	—	—	7.39	—	—	—	—	—	—			
Na_2O	—	—	—	—	0.37	0.69	0.43	0.34	0.29	<0.03	0.03			
K_2O	—	—	—	—	12.3	0.11	0.03	<0.03	0.06	—	—			
La_2O_3	—	—	—	—	—	—	—	—	—	1.15	0.16			
Ce_2O_3	—	—	—	—	—	—	—	—	—	3.32	0.26			
SO_2	—	—	—	—	—	0.21	0.32	<0.05	0.19	—	—			
F	—	—	—	—	—	—	—	—	—	0.28	2.23			
Cl	—	—	—	—	—	—	—	—	—	<0.03	1.69			
Total	99.3	99.8	99.5	100.1	99.7	99.9	100.6	100.0	99.7	89.8	99.7			

Fe-Px = evolved Fe-rich pyroxene; Ilm = ilmenite; Merri = merrillite; FeNi = FeNi metal grain; Min Clast = Monomineralic clast; Agg = Agglutinate; Plag = plagioclase.
Mg# = modal Mg/(Mg + Fe) × 100. Dashed lines indicate elements that were not analyzed.
[a] O_p is the glassy clast O pre-cursor lithology.

Table 4
EMPA and ion microprobe data for Clast A from MET 01210

Mineral	Plagioclase		Plagioclase		Plagioclase		Plagioclase		Plagioclase		Plagioclase		Plagioclase		Merrillite		Merrillite	
Modal %	35.6		35.6		35.6		35.6		35.6		35.6		35.6		0.2		0.2	
Location	G1 Core		G2 Core		G3 Core		G3 Core		G4 Core		G4 Rim		G5 Core		Grain 1		Grain 2	
wt%																		
SiO_2	46.2		45.3		45.1		44.7		45.2		49.7		46.1		0.29		0.32	
Al_2O_3	33.9		33.9		34.1		34.7		34.0		30.6		33.5		—		—	
FeO	0.45		0.59		0.33		0.28		0.48		1.06		0.53		5.07		5.42	
MnO	—		—		—		—		—		—		—		<0.03		<0.03	
MgO	0.09		0.10		0.22		0.18		0.17		0.03		0.11		0.64		0.69	
CaO	18.6		18.7		19.2		19.6		19.0		15.6		18.5		38.2		37.6	
Na_2O	0.80		0.65		0.49		0.35		0.62		1.76		0.99		—		—	
K_2O	0.03		<0.03		<0.03		<0.03		<0.03		0.49		0.05		—		—	
P_2O_5	—		—		—		—		—		—		—		40.9		41.1	
La_2O_3	—		—		—		—		—		—		—		1.15		1.18	
Ce_2O_3	—		—		—		—		—		—		—		3.32		3.18	
F	—		—		—		—		—		—		—		0.28		0.15	
Cl	—		—		—		—		—		—		—		0.03		<0.03	
Total	100.1		99.3		99.4		99.8		99.4		99.3		99.8		89.8		89.6	
An	92.5		94		95.6		96.8		94.2		80.5		90.9		—		—	
p.p.m		±		±		±		±		±		±		±		±		±
Sc	4.1	0.4	4.7	0.3	5.1	0.4	3.2	0.2	3.2	0.2	2.6	0.2	2.8	0.3	—	—	—	—
V	1.8	0.1	3.7	0.2	3.8	0.2	4.2	0.2	3.0	0.1	1.2	0.1	1.7	0.1	—	—	—	—
Cr	2.9	0.2	15.8	0.5	7.3	0.4	8.1	0.3	5.6	0.2	1.7	0.1	3.0	0.2	—	—	—	—
Sr	232	2	201	2	156	2	157	1	200	1	1299	3	242	2	—	—	—	—
Y	0.40	0.03	0.33	0.03	0.46	0.04	0.25	0.02	0.22	0.01	3.50	0.17	0.27	0.02	—	—	—	—
Zr	0.19	0.03	0.22	0.03	0.10	0.02	0.05	0.01	0.12	0.02	8.92	0.32	0.13	0.02	—	—	—	—
Ba	15.1	0.69	10.8	0.47	6.45	0.37	6.44	0.25	9.80	0.33	312	2.33	13.6	0.48	—	—	—	—
La	0.19	0.02	0.15	0.02	0.14	0.02	0.10	0.02	0.17	0.01	2.39	0.12	0.20	0.02	8338	25	8186	34
Ce	0.32	0.03	0.36	0.05	0.24	0.03	0.24	0.02	0.33	0.02	5.60	0.22	0.40	0.03	21988	45	21367	61
Pr	0.05	0.01	0.06	0.01	0.04	0.01	0.03	0.01	0.05	0.01	0.84	0.05	0.08	0.01	2926	14	2815	19
Nd	0.26	0.03	0.23	0.03	0.17	0.03	0.16	0.02	0.18	0.02	2.84	0.10	0.32	0.03	12625	38	12118	52
Sm	0.05	0.03	0.04	0.02	0.12	0.03	0.02	0.01	0.08	0.02	0.74	0.06	0.10	0.03	2764	29	2743	40
Eu	1.70	0.09	1.38	0.07	1.02	0.06	1.07	0.05	1.44	0.06	11.5	0.33	1.77	0.08	169	3	124	4
Gd	0.09	0.02	0.04	0.02	0.08	0.03	0.05	0.01	0.06	0.01	0.68	0.08	0.06	0.02	3288	32	3219	44
Tb	0.02	0.01	0.02	0.01	0.02	0.01	0.01	0.00	0.01	0.00	0.10	0.02	0.02	0.01	611	8	599	11
Dy	0.05	0.02	0.08	0.02	0.10	0.02	0.04	0.01	0.04	0.01	0.67	0.04	0.09	0.02	3312	20	3349	28
Ho	0.01	0.01	0.01	0.01	0.03	0.01	0.01	0.00	—	—	0.22	0.02	0.02	0.01	608	8	612	11
Er	0.02	0.02	0.03	0.01	0.07	0.02	—	—	—	—	0.36	0.03	0.06	0.02	1380	14	1396	19
Tm	—	—	—	—	0.01	0.02	—	—	—	—	0.06	0.04	—	—	134	4	146	5
Yb	0.02	0.02	—	—	—	—	0.02	0.01	0.02	0.01	0.22	0.03	—	—	519	12	591	18
Lu	—	—	—	—	—	—	—	—	0.00	0.00	0.01	0.01	0.00	0.01	32	4	41	6

Table 4 (*continued*)

Mineral	Fe-pyroxene		Pyroxene		Pyroxene		Fe-pyroxene	E	Fe-pyroxene		Pyroxene		Pyroxene		Fe-pyroxene		Fe-pyroxene	
Modal %	6.4		36.8		36.8		6.4		6.4		36.8		36.8		6.4		6.4	
Code	G1 Rim		G1 Core		G1 Core		G1 Rim		G2 Rim		G2 Core		G2 Core		G3		G3	
wt%																		
SiO_2	46.7		50.8		51.9		47.6		48.6		50.6		51.5		47.1		46.6	
TiO_2	0.83		0.72		0.61		0.96		0.89		0.94		0.70		0.97		0.96	
Al_2O_3	0.77		1.44		1.51		0.92		0.96		2.83		1.58		0.94		0.90	
Cr_2O_3	<0.05		0.52		0.60		0.12		0.22		0.97		0.64		0.12		0.06	
FeO	36.2		18.1		16.8		34.4		30.1		14.6		14.4		31.4		37.5	
MnO	0.49		0.35		0.32		0.54		0.44		0.27		0.28		0.54		0.53	
MgO	2.23		13.4		15.3		5.05		8.82		14.3		14.1		5.66		2.33	
CaO	12.0		14.6		13.0		10.3		9.02		15.4		17.0		12.1		11.3	
Na_2O	0.03		0.04		0.03		0.03		0.04		<0.03		<0.03		0.03		<0.03	
Total	99.2		100.0		100.1		100.0		99.1		100.0		100.1		98.7		100.2	
En	7.2		39.4		44.9		15.9		27.4		42.6		40.9		7.4		17.7	
Wo	27.7		30.7		27.4		23.4		20.2		33		35.6		25.9		27.2	
p.p.m		±		±		±		±		±		±		±		±		±
Sc	129	1	111	1	105	1	144	1	125	1	111	1	125	1	146	1	133	1
V	17.1	0.6	140.4	1.4	188.0	1.1	23.8	0.6	99.9	0.8	213.4	1.7	200.4	1.7	21.6	0.5	14.8	0.4
Cr	214	3	4148	11	4856	8	523	3	3233	6	5606	13	5122	12	558	3	308	2
Sr	13.2	0.6	4.7	0.3	4.4	0.2	9.4	0.4	3.2	0.1	3.5	0.2	7.2	0.3	11.2	0.4	13.9	0.4
Y	44.5	0.9	7.0	0.3	7.9	0.2	31.3	0.7	9.6	0.2	7.8	0.3	8.8	0.3	31.1	0.6	50.8	0.7
Zr	28.4	1.1	3.3	0.2	3.5	0.1	21.9	0.8	4.3	0.2	4.9	0.3	4.6	0.2	18.8	0.6	33.6	0.9
Ba	0.19	0.03	0.08	0.01	0.05	0.01	2.82	0.15	0.11	0.02	0.08	0.02	0.10	0.02	0.12	0.02	0.32	0.05
La	0.70	0.07	0.09	0.02	0.08	0.01	0.56	0.05	0.12	0.01	0.17	0.02	0.15	0.02	0.36	0.03	0.63	0.05
Ce	3.69	0.28	0.37	0.04	0.35	0.03	2.48	0.18	0.35	0.02	0.49	0.04	0.70	0.07	1.77	0.11	3.35	0.19
Pr	0.86	0.08	0.09	0.01	0.09	0.01	0.59	0.06	0.09	0.01	0.14	0.02	0.13	0.02	0.40	0.04	0.85	0.06
Nd	5.01	0.25	0.55	0.05	0.67	0.03	3.71	0.18	0.66	0.03	0.68	0.04	1.02	0.06	2.68	0.14	4.35	0.18
Sm	2.47	0.21	0.32	0.04	0.37	0.04	1.86	0.14	0.34	0.03	0.45	0.05	0.45	0.05	1.44	0.12	1.94	0.16
Eu	0.38	0.03	0.06	0.01	0.05	0.01	0.22	0.03	0.04	0.01	0.06	0.01	0.09	0.01	0.15	0.02	0.23	0.02
Gd	3.63	0.40	0.71	3.06	0.70	0.06	3.68	0.34	0.71	0.07	0.65	0.10	0.96	0.11	2.50	0.21	2.98	0.30
Tb	0.89	0.08	0.15	0.02	0.15	0.01	0.68	0.07	0.19	0.02	0.20	0.02	0.21	0.02	0.59	0.05	0.76	0.07
Dy	6.89	0.32	0.96	0.05	1.06	0.04	5.07	0.24	1.52	0.06	1.35	0.08	1.77	0.09	4.09	0.19	6.18	0.24
Ho	1.52	0.11	0.21	0.02	0.25	0.02	0.97	0.10	0.33	0.02	0.36	0.04	0.36	0.03	0.92	0.07	1.20	0.08
Er	4.07	0.21	0.64	0.05	0.73	0.04	3.26	0.16	1.05	0.04	0.88	0.05	1.07	0.06	2.85	0.15	3.81	0.17
Tm	0.52	0.05	0.10	0.01	0.09	0.01	0.42	0.05	0.17	0.01	0.10	0.02	0.14	0.01	0.43	0.04	0.52	0.05
Yb	3.10	0.22	0.74	0.07	0.70	0.05	2.80	0.22	1.19	0.06	0.92	0.08	1.00	0.08	2.67	0.21	3.39	0.22
Lu	0.44	0.08	—	—	0.10	0.02	0.49	0.07	0.16	0.02	0.10	0.03	0.16	0.03	0.48	0.06	0.50	0.07

Errors (±) are one standard deviation of variance in terms of units cited. Dashed lines indicate elements that were not analyzed. G = individual grains of minerals analyzed, some of which were measured for core and rim elemental abundances. An, En and Wo = anorthite, enstatite and wollastonite contents, respectively.

Table 5
EMPA and ion microprobe data for Clast AA from MET 01210

Mineral	Plagioclase		Fayalite		Forsterite		Fayalite		Pyroxene		Pyroxene	
Modal %	71.6		4.7		1.2		4.7		16.4		16.4	
Code	Grain 1		Grain 1		Grain 2		Grain 3		G1 Core		G1 Core	
wt%												
SiO_2	45.4		29.9		33.7		30.6		48.1		47.8	
TiO_2	—		0.11		0.05		0.13		1.38		0.82	
Al_2O_3	33.9		<0.03		<0.03		0.03		1.53		0.87	
Cr_2O_3	—		<0.05		0.13		<0.05		0.15		0.10	
FeO	0.42		66.3		46.9		63.9		27.5		35.3	
MnO	—		0.85		0.53		0.74		0.42		0.52	
MgO	0.26		1.94		18.2		4.12		4.20		6.46	
CaO	19.0		0.82		0.38		0.69		16.7		7.46	
Na_2O	0.50		—		—		—		0.03		0.03	
K_2O	0.03		—		—		—		—		—	
Total	99.5		100.0		100.0		100.2		100.1		99.4	
An	95.3		—		—							
Fo	—		5.0		41.0		10.3					
En	—		—		—		—		13.3		20.4	
Wo	—		—		—		—		37.9		16.9	
p.p.m		±		±		±		±		±		±
Sc	2.8	0.4	12.2	0.2	17.6	0.2	19.5	0.3	260	1	184	1
V	4.9	0.3	0.9	0.1	32.1	0.4	1.8	0.1	32.6	0.7	30.7	0.7
Cr	7.8	0.4	58.5	0.7	1259	3	126.1	1.1	1297	6	1308	6
Sr	150	2	0.48	0.04	0.2	0.0	0.5	0.0	21.7	0.6	9.9	0.5
Y	0.30	0.02	21.8	0.4	1.4	0.1	8.5	0.2	43.7	0.8	30.6	0.7
Zr	0.20	0.04	2.6	0.1	0.1	0.0	0.7	0.0	50.6	1.3	22.1	0.8
Ba	7.6	0.4	0.34	0.04	0.14	0.02	0.29	0.03	0.17	0.04	0.17	0.03
La	0.16	0.02	—	—	—	—	—	—	0.91	0.08	0.36	0.04
Ce	0.38	0.04	—	—	—	—	—	—	3.94	0.27	1.54	0.13
Pr	0.05	0.01	—	—	—	—	—	—	0.81	0.07	0.42	0.04
Nd	0.20	0.03	0.12	0.01	—	—	0.10	0.01	5.96	0.26	2.87	0.14
Sm	0.05	0.03	0.12	0.02	0.02	0.1	0.05	0.01	2.67	0.23	1.15	0.13
Eu	1.07	0.08	0.00	0.00	0.00	0.00	0.00	0.00	0.29	0.03	0.14	0.02
Gd	0.04	4.2	0.42	0.04	0.05	0.01	0.25	0.03	4.20	0.47	2.54	0.26
Tb	—	—	0.17	0.01	0.02	0.00	0.09	0.01	0.93	0.11	0.50	0.05
Dy	0.07	0.02	2.04	0.07	0.16	0.01	0.94	0.04	6.66	0.33	4.74	0.21
Ho	0.01	0.01	0.63	0.04	0.04	0.00	0.28	0.02	1.30	0.11	0.76	0.07
Er	0.03	0.01	2.88	0.09	0.16	0.01	1.04	0.05	4.20	0.22	2.77	0.15
Tm	—	—	0.50	0.04	0.03	0.00	0.20	0.02	0.64	0.05	0.37	0.04
Yb	—	—	3.77	0.19	0.22	0.02	1.44	0.07	3.29	0.31	2.82	0.20
Lu	0.00	0.01	0.70	0.05	0.05	0.01	0.24	0.02	0.59	0.09	0.46	0.07

Errors (±) are one standard deviation of variance in terms of units cited. Dashed lines indicate elements that were not analyzed. G = individual grains of minerals analyzed, some of which were measured for core and rim abundances. An, Fo, En and Wo = anorthite, forsterite, enstatite and wollastonite contents, respectively.

immature polymict, predominantly basaltic, fragmental breccia. Due to the presence of agglutinates and glass, the meteorite can be further classified as an immature, predominantly basaltic glassy-matrix regolith breccia. The polished section studied is composed of lithic clasts of basalt (⩽3 mm) and granulitic anorthosite, as well as symplectic fragments and mineral clasts of angular pyroxene, plagioclase, olivine and Fe–Ti oxide set in a matrix of predominantly glassy material (Fig. 1). As a whole, the breccia contains ~35 vol % olivine and pyroxene, ~65 vol % plagioclase, silica and matrix and ~1 vol % oxides, troilite and FeNi metal. The regolith component is restricted to a few rounded agglutinates, although some 'regolith spheroids' have been reported (Huber and Warren, 2005).

3.1.1. Basaltic clasts

Basalt fragments make up ~70 vol % of the lithic clast population in MET 01210. Basaltic clasts possess a wide range of textures and mineralogies (Table 1). The textures range from relatively coarse-grained (length = 0.5–1.0 mm) intergranular (clast A) to fine-grained (⩽0.5 mm) subophitic (clast AA), to very fine-grained (⩽0.1 mm) plumose (clast K) (Fig. 1a–c). The largest clast, clast A (3.0 × 2.5 mm), is predominantly composed of strongly zoned pyroxene grains with compositions from Mg-pigeonite ($Wo_{21}En_{49}$) to pyroxferroite (Wo_1En_3) (Tables 2 and 3; Fig. 2a). Plagioclase grains in clast A range from An_{97} to An_{80}, with the most sodic examples (up to 1.6 wt% Na_2O) associated with a single mesostasis area preserved

Table 6
Representative EMPA data for glasses in MET 01210 and PCA 02007

Type	MET 01210 Agglutinate		MET 01210 Agglutinate		PCA 02007 Agglutinate		PCA 02007 Spherule[a]		PCA 02007 Spherule		PCA 02007 Spherule[b]	
Clast I.D.	O		$O^{c}_{included}$		T13		T3		T20a		T48	
n	15		5		5		6		10			
wt%	Average	1 SD	Average	1 SD	Average	1 SD	Average	1 SD	Average	1 SD	Average	1 SD
SiO_2	45.0	1.4	48.3	3.0	43.3	0.8	41.2	0.2	46.2	0.1	45.1	0.8
TiO_2	1.19	0.52	0.36	0.04	0.29	0.03	0.30	0.03	1.06	0.04	0.28	0.06
Al_2O_3	16.3	4.1	18.0	1.7	24.7	0.4	26.7	0.1	15.8	0.1	24.3	2.4
Cr_2O_3	0.22	0.06	0.39	0.15	0.17	0.05	0.11	0.03	0.33	0.05	0.17	0.04
FeO	15.6	4.6	10.6	1.3	6.44	0.33	6.62	0.07	14.3	0.4	6.28	3.36
MnO	0.24	0.08	0.20	0.03	0.10	0.02	0.10	0.02	0.20	0.02	0.11	0.04
MgO	6.62	1.02	8.71	0.43	7.16	0.11	7.51	0.07	7.99	0.08	7.70	1.72
CaO	13.2	0.7	12.7	0.9	15.1	0.1	16.0	0.1	12.5	0.1	14.7	1.3
Na_2O	0.29	0.09	0.40	0.07	0.26	0.04	0.05	0.02	0.19	0.03	0.31	0.06
K_2O	0.04	0.02	0.03	0.01	<0.03		<0.03		<0.03		<0.03	
P_2O_5	0.19	0.03	0.17	0.05	0.03	0.01	0.04	0.02	0.04	0.01	0.03	0.02
SO_2	—	—	—	—	0.09	0.02	<0.05		0.08	0.02	0.07	0.04
BaO	—	—	—	—	—	—	<0.03		0.03	0.04	<0.03	
Total	98.9		99.9		97.7		98.5		98.8		99.2	
Mg#	43.1		59.3		66.5		66.9		49.9		68.6	

[a] Contains inclusion with glass-plagioclase (An_{95})-pyroxene-olivine (Fo_{80}) assemblage.
[b] Contains plumose textures though no stoichiometric minerals.
[c] Pre-cursor agglutinate included within the major mass of glassy fragment clast O. Mg# = molar Mg/(Mg + Fe) × 100. Dashed lines indicate elements that were not analyzed.

within the clast. Ulvöspinel (molar Cr/(Cr + Ti) × 100 = 6–20) and ilmenite (MgO = 0.2–0.4 wt%) are included within the Fe-rich rims of zoned pyroxene grains. Symplectic textures, where pyroxferroite has broken down to hedenbergite ($Wo_{40}En_{6-10}$), fayalite (Fo_{3-7}) and silica, occurs with ilmenite, troilite, K-rich glass and merrillite (~50 × 20 μm; 2.9–3.3 wt% Ce_2O_3) within the mesostasis areas. Clast A appears to be similar in nature to the coarse-grained basaltic clast described by Arai et al. (2005) for MET 01210.

Clast AA is a subophitic basalt with tabular crystals of plagioclase (0.3–0.4 mm in length) that have a restricted range of anorthite contents ($An_{94\pm2}$), and olivines that are more forsteritic (Fo_{6-41}) than those documented in clast A (Tables 2 and 3). Pyroxene compositions in clast AA are more Fe-rich than for some of the core compositions in clast A (Fig. 2a). The other major basalt clast identified is clast K, a 'plumose' or feathery textured basalt, much like the texture exhibited in the groundmass of NWA 032 (e.g., Fagan et al., 2002). Clast K has a slightly more restricted range of pyroxene compositions than clast A, from augite to ferroaugite (Fig. 2a). Two coarse grained lithic clasts in MET 01210 (BB and H) are remnants of extremely Fe-enriched basaltic precursors, with ferroaugite to pyroxferroite pyroxene compositions. These clasts also contain skeletal ilmenite and evolved late stage crystallization products (e.g., silica, ulvöspinel), and are similar to the opaque-rich clasts of Arai et al. (2005).

In general, the basaltic clasts in MET 01210 are low- to very-low titanium in composition and have undergone extreme fractionation from their parental melt compositions. These basalt clasts are more Fe-rich than those found in a number of basaltic and predominantly basaltic breccia meteorites (EET 87521/96008, QUE 94281, Y-793274, Y-793169 and A-881757; Jolliff et al., 1998; Anand et al., 2003 and references therein), but appear similar to some recently described from the brecciated portion of NWA 773 (Fagan et al., 2003), and to some evolved basaltic lunar meteorites (NWA 032; LAP 02205/02224/02226/02436 and LAP 03632—the LaPaz basalts; Fagan et al., 2002; Day et al., 2006; Zeigler et al., 2005b). Pyroxene crystallization histories are also similar to the low titanium/very low titanium basaltic lunar meteorites. In a pioneering study, Bence and Papike (1972) outlined how mineral chemistry of lunar pyroxenes recorded the crystallization of plagioclase and Ti-rich oxides that affect Tschermak-titanian substitutions. Bence and Papike (1972) further considered that these relations, best expressed in Ti (afu)–Al (afu) space, would allow basic crystallization histories to be deduced for small lithic and mono-mineralic fragments. Ti/Al relations for pyroxenes from basaltic lithic clasts of MET 01210 are presented in Fig. 3 along with the chemical trends of an analog pyroxene crystallization experiment for an Apollo 15 mare basalt (15597; Grove and Bence, 1977).

According to the interpretations of pyroxene mineral chemistry by Bence and Papike (1972) and, more recently, Arai et al. (1996), basaltic fragments BB, H and AA indicate continuous crystallization of pyroxenes, with Ti/Al = ~0.5, consistent with pyroxene and plagioclase co-crystallization. Clast A first underwent crystallization of Mg-pigeonites with low Ti and Al and Ti/Al = 0.25 progressing to more Ti and Al-rich augites. The sub-calcic augite population in clast A have Ti/Al = 0.5 indicating the onset of plagioclase crystallization. Continued crystallization of the clast A parental magma resulted in more Fe-rich

Table 7
Representative EMPA data for silicate, oxide, phosphate and accessory phases in PCA 02007

Phases	Pyroxene	Pyroxene	Pyroxene	Pyroxene	Pyroxene	Fe-Px	Fe-Px	Olivine	Olivine	Fayalite	Plag	Plag	Plag	Plag
Sample	Clast ZD	Clast T38	Clast T2	Clast F	Min Clast	Clast T35	Clast T35	Clast T38Cl	Clast W	Min Clast	Clast T35	Clast Tl	Clast E	Min Clast
wt%														
SiO_2	55.3	51.2	53.0	51.3	48.8	45.3	44.1	38.8	40.2	29.7	45.3	43.9	43.9	49.5
TiO_2	0.60	0.96	0.64	1.41	0.58	1.65	2.20	0.05	0.03	0.10	—	—	—	—
Al_2O_3	1.11	0.95	0.90	1.48	1.14	1.46	1.44	0.03	0.03	<0.03	33.2	34.9	35.2	31.1
Cr_2O_3	0.31	0.37	0.33	0.36	0.49	0.16	<0.05	0.14	0.07	<0.05	—	—	—	—
FeO	10.4	21.5	18.6	12.6	29.5	36.4	40.6	19.5	12.9	66.1	0.76	0.33	0.31	0.59
MnO	0.18	0.36	0.34	0.25	0.50	0.48	0.48	0.20	0.19	0.85	—	—	—	—
MgO	30.7	19.4	24.1	16.0	10.1	3.05	0.29	41.1	46.9	2.25	0.24	0.18	0.08	0.10
CaO	1.25	4.84	2.03	16.1	8.81	11.0	10.2	0.17	0.08	0.67	19.3	19.3	19.5	15.1
Na_2O	<0.03	<0.03	<0.03	0.12	0.03	<0.03	<0.03	—	—	—	0.49	0.47	0.31	2.59
K_2O	—	—	—	—	—	—	—	—	—	—	<0.03	<0.03	<0.03	0.29
Total	99.9	99.6	99.9	99.6	99.9	99.5	99.3	99.9	100.4	99.7	99.3	99.0	99.3	99.0
Mg#	84.0	61.7	69.8	69.5	38.0	13.0	1.2	78.9	86.6	5.7	An = 95.5	An = 95.8	An = 97.1	An = 75.0

Phases	Spinel	Spinel	Ilm	Ilm	Glass	Glass	Glass	Glass	Glass	Glass	Glass		FeNi	FeNi
Sample	Min Clast	Min Clast	Clast X	Min Clast	Vol Sph	Vol Sph	Melt Sph	Plag Sph	Plag Sph	Plag Sph	Agg		Matrix	Clast T2
wt%														
SiO_2	0.80	0.05	0.11	<0.03	44.6	45.9	46.9	44.1	43.8	45.3	44.0	Fe	89.6	98.5
TiO_2	17.8	0.22	52.1	52.8	0.46	1.01	0.60	0.26	0.24	0.34	0.35	Co	0.18	0.17
ZrO_2	—	—	—	0.14	—	—	—	—	—	—	—	Ni	3.99	1.40
Al_2O_3	6.71	59.8	0.18	0.03	15.9	15.8	17.6	23.1	29.3	23.0	25.2	P	2.74	0.07
V_2O_3	0.56	0.06	—	—	—	—	—	—	—	—	—	S	3.27	<0.05
Cr_2O_3	25.8	3.95	0.39	0.25	0.40	0.28	0.34	0.28	0.09	0.14	0.14	Si	<0.03	0.03
FeO	42.4	22.6	45.6	46.7	13.0	15.3	12.7	9.36	4.38	7.06	6.70			
MnO	0.28	0.16	0.37	0.48	0.19	0.25	0.21	0.09	0.09	0.10	0.07			
MgO	4.25	12.7	0.86	0.14	14.0	8.03	8.38	7.39	4.97	7.38	6.83			
CaO	1.05	0.06	0.11	0.06	10.2	12.4	12.3	14.4	16.7	16.0	15.3			
BaO	—	—	—	—	<0.05	<0.05	<0.05	0.05	<0.05	0.05	<0.05	Total	99.8	100.2
Na_2O	—	—	<0.03	—	0.25	0.16	0.27	0.30	0.13	0.24	0.33			
K_2O	—	—	—	—	<0.03	<0.03	<0.03	<0.03	<0.03	<0.03	0.09			
SO_2	—	—	—	—	<0.05	0.07	0.26	0.53	<0.05	0.12	0.19			
Total	99.6	99.6	99.7	100.6	99.1	99.2	99.6	99.9	99.7	99.7	99.2			

Abbreviations: Fe-Px = Evolved Fe-rich pyroxene; Ilm = ilmenite; FeNi = FeNi metal grain, Min Clast = Monomineralic clast; Vol Sph = basaltic glass bead?; Melt Sph = Melt sphere; Plag Sph = Plagioclase-rich sphere; Plag = Plagioclase. Mg# = molar $Mg/(Mg + Fe) \times 100$. An = Anorthite content (molar $Ca/(Ca + Na + K) \times 100$). Dashed lines indicate elements that were not analyzed.

Table 8
Representative EMPA and ion microprobe data for meteorite clast T8, PCA 02007

	Glass 1		Glass 2		Glass 3		Olivine 1		Olivine 2		Olivine 3		Plag 1		Plag 2	
wt%																
SiO_2	43.6		42.3		43.8		41.8		38.7		39.3		47.0		48.1	
TiO_2	1.22		1.22		1.20		<0.03		<0.03		<0.03		—		—	
Al_2O_3	9.00		10.6		8.57		<0.03		0.13		0.14		31.8		32.0	
Cr_2O_3	0.09		<0.05		0.07		0.60		0.37		0.26		—		—	
FeO	22.0		21.1		23.2		1.49		18.2		15.5		1.21		1.24	
MnO	0.32		0.30		0.37		0.19		0.17		0.19		—		—	
MgO	0.75		0.85		0.56		55.8		42.2		44.8		0.27		0.25	
CaO	18.2		18.3		17.7		0.25		0.26		0.27		16.3		16.1	
Na_2O	0.94		0.97		0.89		—		—		—		1.96		2.21	
K_2O	0.41		0.27		0.44		—		—		—		0.05		0.04	
P_2O_5	1.10		1.12		0.96		—		—		—		—		—	
SO_2	1.12		1.38		1.33		—		—		—		—		—	
Total	98.7		98.5		99.0		100.1		100.1		100.4		98.6		99.9	
Mg#	5.7		6.7		4.1		98.5		80.5		83.8					
p.p.m		±		±		±		±		±		±		±		±
Sc	22.6	5	18.1	5	25.8	5	11.7	5	16.1	5	12.4	4	13.3	4	13.7	5
V	191	2	56.7	9	89.4	10	32.7	9	80.2	10	69.4	1	62.9	9	50.3	8
Rb	7.9	13	6.2	13	5.6	11	0.9	3	2.3	9	2.4	7	1.6	7	1.9	7
Sr	65.4	11	61.5	11	51	8	1.6	1	32.5	7	15.7	4	105.3	13	88.5	11
Y	10.3	4	8.1	3	14.8	5	0.66	3	4.9	2	3.0	2	3.9	2	3.8	2
Zr	33.7	10	23.7	8	35.3	8	1.5	1	16.1	6	12.3	3	12.9	5	8.3	4
Ba	16.5	8	11.7	7	18.0	6	1.1	1	11.8	6	2.6	2	8.9	5	8.2	4
La	2.1	1	1.6	1	3.4	2	—	—	1.11	8	1.01	8	0.83	6	0.91	7
Ce	4.4	2	3.5	2	8.3	3	0.20	2	2.60	2	1.32	7	1.8	1	2.2	1
Pr	0.73	5	0.50	5	1.19	6	0.04	1	0.46	4	0.31	3	0.31	2	0.33	3
Nd	3.1	1	2.4	1	5.6	2	0.26	3	1.1	8	1.12	6	1.14	8	1.36	8
Sm	0.86	8	0.58	7	1.8	1	0.26	3	0.46	6	0.26	4	0.39	6	0.34	6
Eu	0.35	4	0.25	2	0.65	4	0.02	1	0.18	2	0.09	1	0.39	3	0.49	4
Gd	1.1	1	0.7	1	2.3	2	0.09	3	0.39	9	0.24	5	0.48	7	0.47	8
Tb	0.22	3	0.13	2	0.42	3	0.01	1	0.13	2	0.07	1	0.10	1	0.11	2
Dy	1.45	8	0.82	6	2.7	1	0.07	2	0.78	4	0.38	3	0.60	4	0.65	5
Ho	0.31	3	0.22	2	0.56	3	0.02	1	0.20	3	0.10	1	0.12	2	0.11	2
Er	0.96	5	0.63	5	1.83	8	0.06	2	0.53	4	0.27	3	0.38	3	0.38	4
Tm	0.15	2	0.09	1	0.28	3	0.01	1	0.09	2	0.02	1	0.05	1	0.04	1
Yb	0.97	7	0.55	7	1.5	1	0.08	3	0.62	5	0.23	4	0.37	4	0.36	5
Lu	0.13	2	0.08	2	0.23	3	—	—	0.07	2	0.06	2	0.06	2	0.04	1

Errors (±) are one standard deviation of variance in terms of units cited. Mg# = molar Mg/(Mg + Fe) × 100. Dashed lines indicate elements that were not analyzed.

compositions with Ti/Al = ~1 suggesting late-stage co-crystallization of ulvöspinel, plagioclase and pyroxene (Fig. 3). Clast K possesses a similar trend to clast A, although augites and sub-calcic augites are more Ti- and Al-rich, due to the rapid quenching of this clast (20–60 °C/h; Lofgren et al., 1974). Lofgren et al. (1974) argued that rapidly cooled crystals have preferential uptake of Ca–Fe–Al–Ti relative to Mg–Si in the pyroxene lattice.

We determined the trace element abundances of basalt clasts A and AA by ion probe analysis of major silicate phases (Tables 4 and 5, Fig. 4a–c). Pyroxene, plagioclase and olivine, observed from EMPA to span a range of mineral compositions, were analyzed, as well as two merrillites from the mesostasis in clast A. Using this data, we determined modal recombinations of clast 'whole-rock' trace element compositions to provide a quantitative measure of the parental melt compositions of clasts, allowing comparison with previously studied mare basalts. Pyroxenes in clast A and AA preserve primary igneous zonation and show compatibility of Sc, Cr and V and incompatibility of Zr and Y with increasing fractionation (Tables 4 and 5). REE abundances of pyroxenes also increase with increasing fractional crystallization of the parental melt of the clasts, with ferro-augites having similar REE patterns to augite, but higher absolute REE concentrations (Fig. 4a). Pyroxenes in clasts A and AA have REE patterns and abundances, which in general terms, are similar to those measured in LaPaz low-Ti evolved mare basalt meteorites, and which have been plotted in Fig. 4a for comparative purposes.

Because olivines in clast A were volumetrically insignificant, only olivines in clast AA were selected for analysis by ion microprobe. The olivine REE patterns are consistent with fractionation, with increasing heavy REE (HREE), and decreasing compatible element abundances with increasing fayalite content; the HREE enrichments are greater than those of other evolved mare basalts (Table 5;

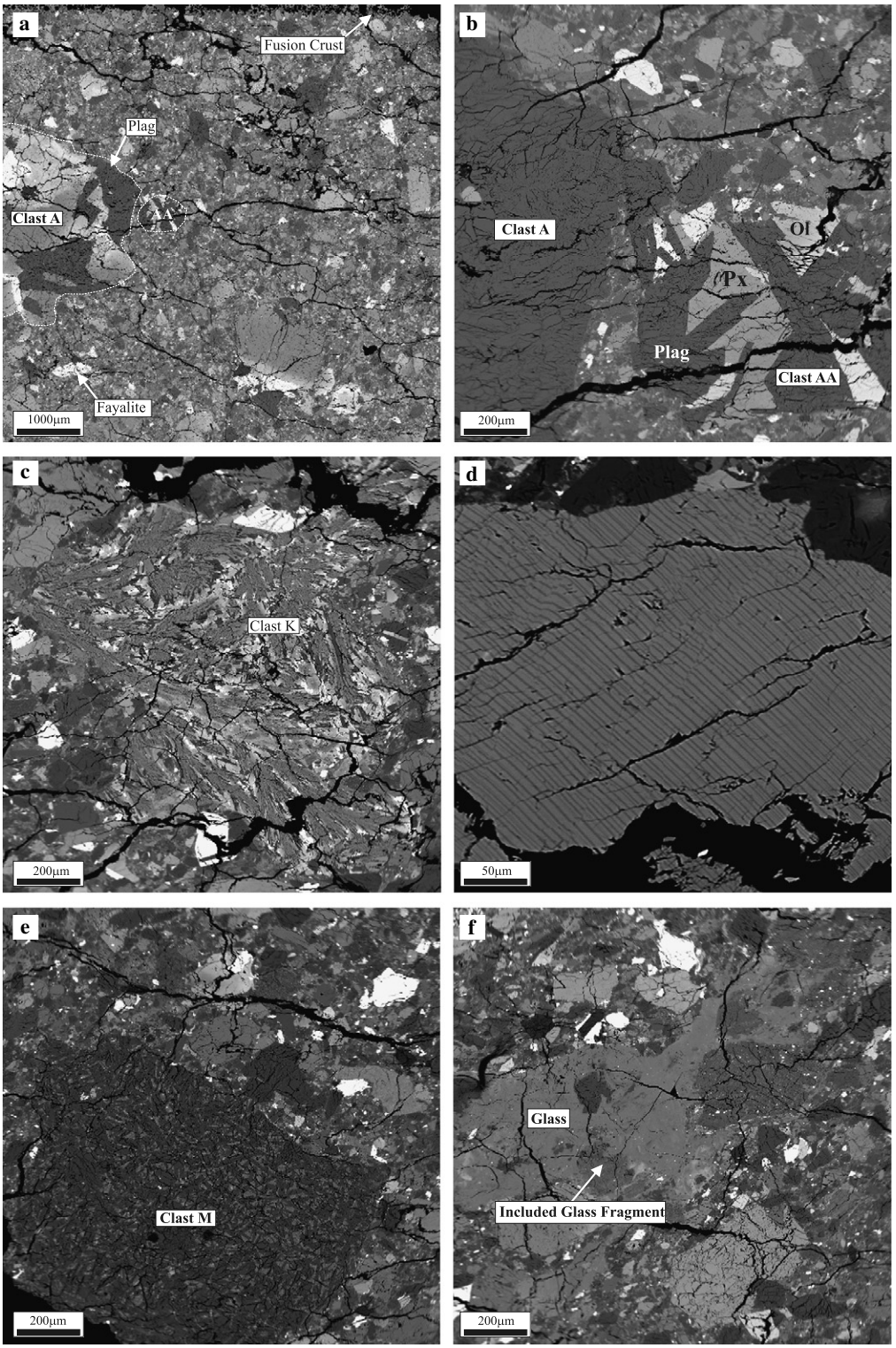

Fig. 1. Back-scattered electron (BSE) images of textural features in MET 01210. (a) BSE image of the major portion (~70%) of the polished section examined in this study illustrating the brecciated nature of the meteorite. Dark grey = plagioclase, intermediate grey = olivine and pyroxene, and light grey = ilmenite, fayalite and spinel. A vesiculated fusion crust surrounds the meteorite (at the top of image) and clast A takes up the left-most, centre portion of the image. Other notable features include the large fayalite mineral clast (bright, irregular outline) at the lower left-hand corner of the image, and the obvious zonation in the pyroxenes within clast A and the pyroxene clast in the lower right-hand corner of the image. (b) BSE image of clast AA, next to coarser grained clast A, showing the subophitic texture of this basaltic fragment. Other notable clasts include: (c) the plumose textured basaltic clast K; (d) a large exsolved pyroxene in a coarse grained basaltic fragment; (e) plagioclase-rich meta-melt clasts similar to those found in mixed basaltic regolith breccias (e.g., QUE 93069; Koeberl et al., 1996) and (f) a glassy clast and surrounding mineral clasts within the breccia. Note differences in scales and the fragmented nature of individual clasts within the BSE images.

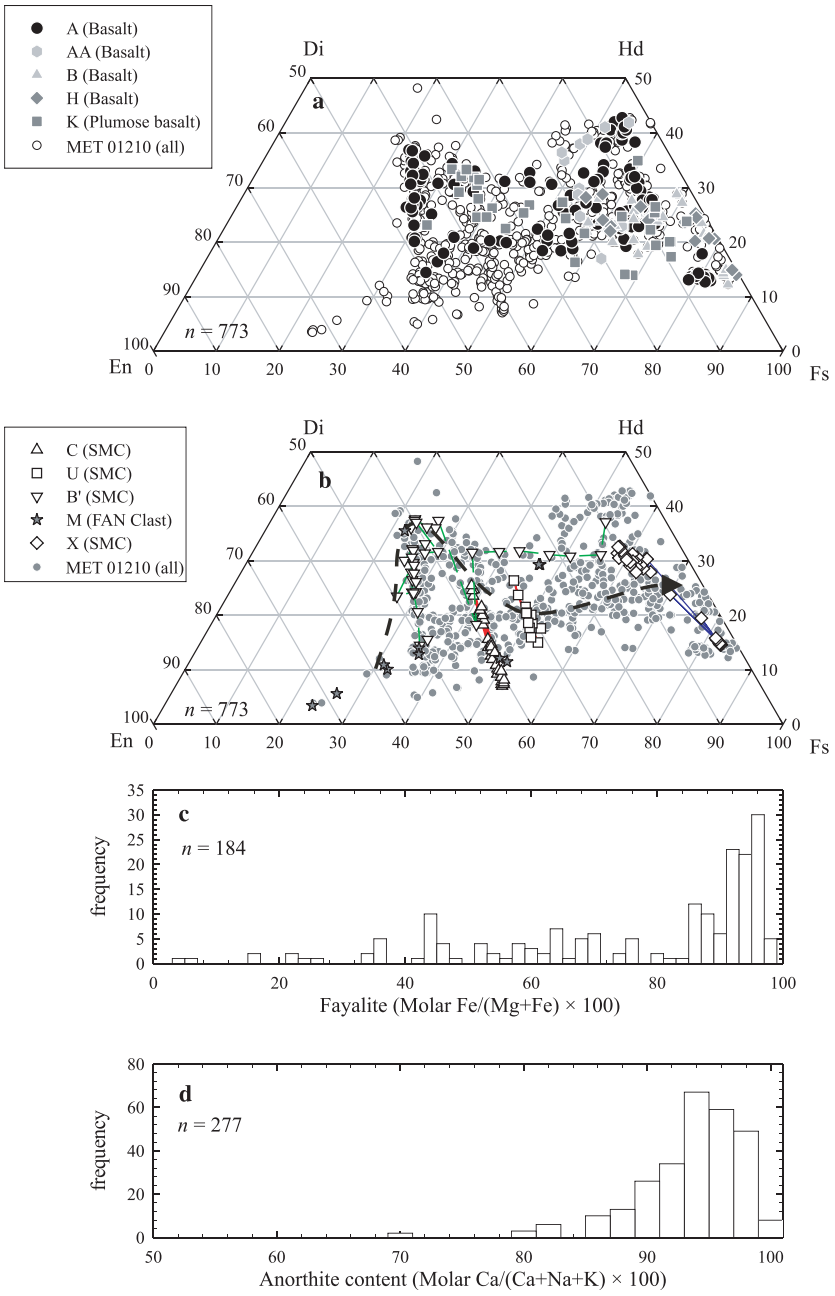

Fig. 2. Pyroxene, olivine and plagioclase compositions for selected lithic and mineral clasts in MET 01210. Unshaded and grey shaded circles in (a and b) respectively are data points obtained on all pyroxenes in MET 01210 during the course of this study. (a) Pyroxene quadrilateral for basaltic lithic clasts. Compositions of pyroxenes in the basaltic clasts (e.g., A, K) cover nearly the entire range of pyroxene compositions measured in MET 01210 (e.g., clast M). (b) Pyroxene quadrilateral for feldspathic clasts (described as 'ferroan anorthosite' or FAN) and single mineral clasts (SMC). The 'tail' of high Mg low Ca pyroxene compositions are entirely accounted for by the populations of feldspathic clasts in MET 01210. Compositions of pyroxenes are compared with zoning trends in pyroxenes from experiments on lunar basalt 15597 (dashed arrowed line—Grove and Bence, 1977). (c) Olivine compositions for MET 01210 illustrating the preponderance of fayalitic olivines in the sample; forsteritic olivines are restricted to mineral clasts and do not occur in basaltic clast fragments. (d) Plagioclase compositions for MET 01210 with a tail to low anorthite compositions associated with the closed-system fractionation of basaltic clast precursor magmas and complementary enrichment in incompatible elements.

Fig. 4b). In general, plagioclase in the clasts spans a limited range of anorthite contents. A single grain of An_{80} plagioclase has higher Sr and Ba abundances (Table 4) than the other plagioclase grains. This grain also has higher REE abundances than the other grains, although its REE pattern is similar; higher REE abundances are typical for lunar plagioclases that form late in the crystallization sequence (Fig. 4c). Like previous ion microprobe studies of lunar basaltic meteorites (e.g., Jolliff et al., 1993; Anand et al., 2003; Anand et al., 2006), we find that phosphates in the mesostasis of clast A have elevated abundances of the REE (Table 4; Fig. 4c). Merrillites in clast A have somewhat steeper HREE-depleted patterns relative to merrillites in the LaPaz mare basalts and in EET 96008 (Fig. 4c); variations in mer-

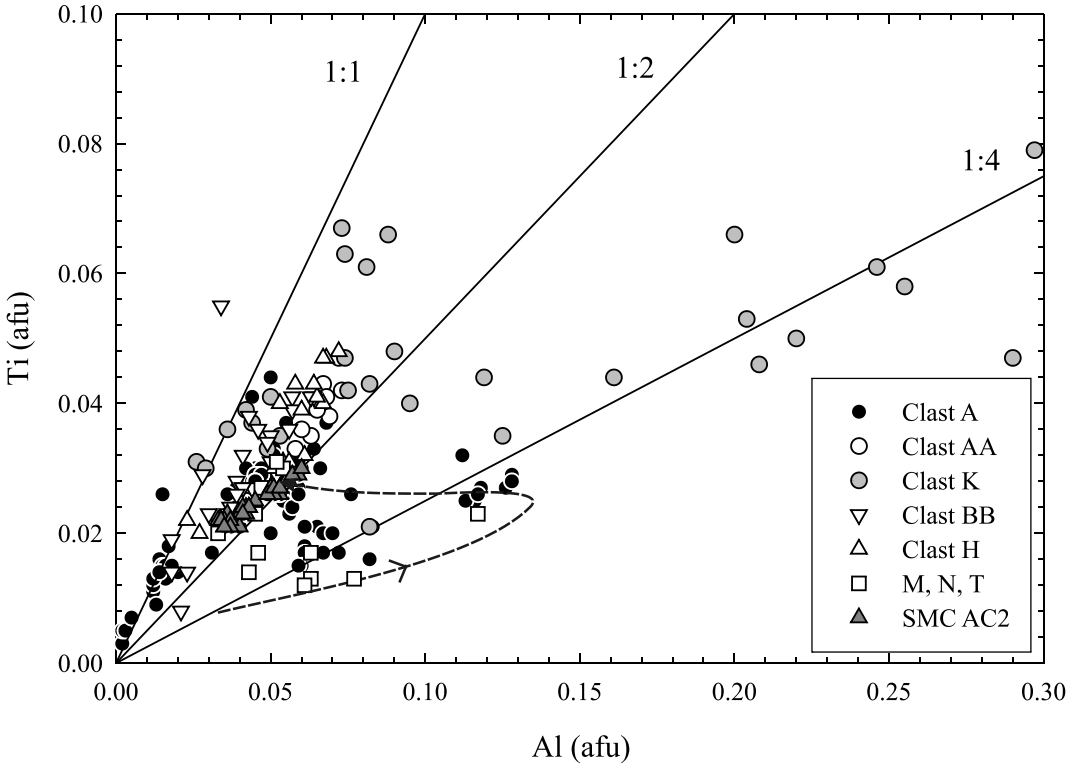

Fig. 3. Pyroxene compositions for lithic clasts in MET 01210 as a function of Ti and Al (atomic formula units—afu). Data are compared with pyroxene crystallization experiments from Grove and Bence (1977). Decrease in Al, relative to Ti, marks the onset of plagioclase crystallization. Lines denoted 1:1, 1:2, 1:4 indicate ratios of Ti/Al = 1, 0.5 and 0.25, respectively.

rillite REE patterns have also been noted by Neal and Taylor (1991 and references therein).

Previous studies have demonstrated the close correspondence between whole-rock trace element compositions measured on homogenized powder aliquots of mare basalts and whole-rock recombinations of the same samples by using modal data and mineral REE compositions (e.g., Anand et al., 2006). Whole-rock modal recombination of clasts A and AA yield HREE-depleted and HREE-enriched patterns, respectively (Fig. 4d), and are unlike the REE patterns of typical mare basalts. Recombination of whole-rock compositions using modal data and mineral trace element data show the significance of phosphate for determining accurate bulk REE compositions. A modal recombination using only the silicate minerals analyzed in clast AA results in a light REE (LREE) depleted whole-rock composition (Fig. 4d). However, using the phosphate data of clast A (Table 4), a LREE-enriched whole-rock composition similar to that of clast A is reconstructed (Fig. 4d). Clast size also significantly affects modal recombination, especially if minerals within the clast are coarse grained. With these caveats in mind, we do not place emphasis on whole-rock compositional constraints for these clasts and note that minor minerals (phosphate, zirconium-rich minerals) have important controls on trace element abundances in these modal recombinations.

3.1.2. Feldspathic clasts

Feldspathic clasts make up the remaining ~30 vol % of the lithic clast inventory in MET 01210. The textures of these clasts are invariably granulitic (Fig. 1e) and the mineralogy is dominantly that of anorthosite (Tables 1–3). Pyroxenes in the feldspathic clasts range from orthopyroxene to sub-calcic augite (Fig. 2). These feldspathic clasts probably have an impact melt origin, however, their pyroxenes possess Ti/Al which record plagioclase crystallization and separation. For example, orthopyroxene is characterized by Ti/Al = ~0.25 indicating crystallization in a liquid saturated in Al, whereas the more evolved clinopyroxenes possess Ti/Al = ~0.5, possibly representing late stage crystallization after the separation of plagioclase within these clasts (Fig. 3). The feldspathic clasts also contain FeNi metal grains (0.2–0.6 wt% Co; 5.5–15.5 wt% Ni) similar to those reported in meta-melt clasts from QUE 93069, a feldspathic regolith breccia (Koeberl et al., 1996); these metals almost certainly have an exogenous (i.e., meteoritic) origin. The feldspathic clasts in MET 01210 have similar textures and plagioclase/mafic mineral ratios as granulite clasts in QUE 93069 and MAC 88105, which are considered to have experienced thermo-metamorphic recrystallization (Koeberl et al., 1991, 1996).

3.1.3. Agglutinitic glass

A single relatively large, ropy clast (~0.9 × 0.5 mm) and some smaller fragments of agglutinate were recognized in

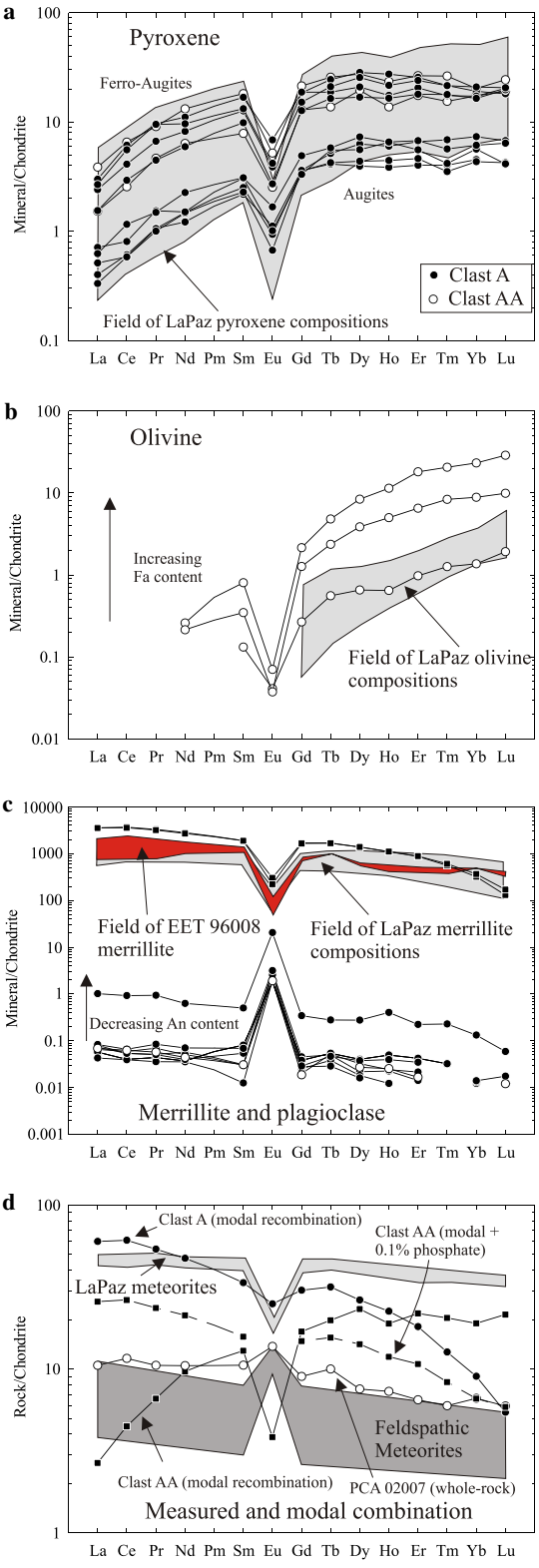

Fig. 4. CI chondrite-normalized REE abundances in (a) pyroxene, (b) olivine, (c) merrillite and plagioclase from clast A and AA of MET 01210 and (d) of whole-rock compositions for PCA 02007 and estimated whole-rock recombinations for clast A and clast AA in MET 01210. Also shown in (d) is the typical measured range of REE in whole-rock feldspathic meteorite breccia analyses (from Korotev et al., 2003) and in evolved mare basalt meteorites (Day et al., 2006). The gap between ferro-augite and augite compositions in (a) is likely the result of sampling. Normalization data from Anders and Grevesse (1989).

MET 01210. The largest glassy clast (O) is characterized by discontinuous schlieren that contains plagioclase fragments ($An_{90–96}$), sub-micrometer Fe^0 particles, as well as two fragments of possible precursor vitrophyric material (Table 3). The compositions of the precursor vitrophyric fragments are more homogenous than the agglutinitic glass and have MgO contents of ~5 and 9 wt%, respectively (Tables 3 and 6; Fig. 5). The composition of the agglutinate is less Al_2O_3-rich than similar agglutinitic clasts within predominantly basaltic breccia NWA 773 (Fagan et al., 2003), or in feldspathic breccias such as PCA 02007 (Fig. 5).

3.1.4. Mineral clasts and matrix material

Pyroxene is the predominant mineral clast type in MET 01210. A small proportion of pyroxenes clasts are high-Mg-pigeonites, and are preserved within lithic feldspathic clasts (Section 3.1.2). The majority of minerals clasts have pyroxene compositions more typical of mare basalt chemistries (Fig. 2b). Some pyroxene clasts within MET 01210 are exsolved with relatively wide exsolution lamellae (average width = 2.4 μm) and have Ti/Al ratios = 0.5, consistent with concomitant plagioclase fractionation (Fig. 3). The average width of the exsolution lamellae for MET 01210 pyroxene grains are similar to those measured in other anorthosite-bearing fragmental basalt breccias Y-793274 (~0.35–>1 μm), QUE 94281 (~1–>2 μm) and paired meteorites EET 87521 and EET 96008 (~500–>1 μm); wide exsolution lamellae are considered indicators of slow cooling (e.g., Jolliff et al., 1998; Arai and Warren, 1999; Anand et al., 2003), although they have not been recognized in relatively slow cooled basalt meteorites such as the LaPaz basalts (Day et al., 2006). It should be noted that the orientation of sectioning through an exsolved pyroxene has a significant impact on the average width of the exsolution lamellae so that the average width should probably be considered a maximum. Traverses of pyroxene exsolution indicate crystallization temperatures in the range of 1100–1200 °C and equilibration temperatures that extend no lower than ~900 °C based on the two-pyroxene thermometer of Lindsley and Andersen (1983).

Fragments with symplectic breakdown textures are present as individual clasts within MET 01210, as well as within the mesostasis of Clast A. These vermicular symplectic textures consist of fayalite ($Fo_{3–6}$), hedenbergite ($Wo_{40}En_{6–10}$) and silica and are characteristic of original pyroxene compositions that are Fe-rich ($Wo_{15}En_4$–$Wo_{15}En_8$—measured using defocused beam analysis). Similar symplectites have been recognized in a number of basaltic breccias (Jolliff et al., 1998; Fagan et al., 2003) and occur when metastable pyroxenoids (e.g., pyroxferroite) are slowly cooled, resulting in break-down to fayalite + hedenbergite + silica (Lindsley et al., 1972).

Monomineralic olivine clasts have compositional ranges spanning almost the entire spectrum of forsterite contents (Fo_{94} to Fo_1) (Fig. 2c). Forsteritic grains occur as small

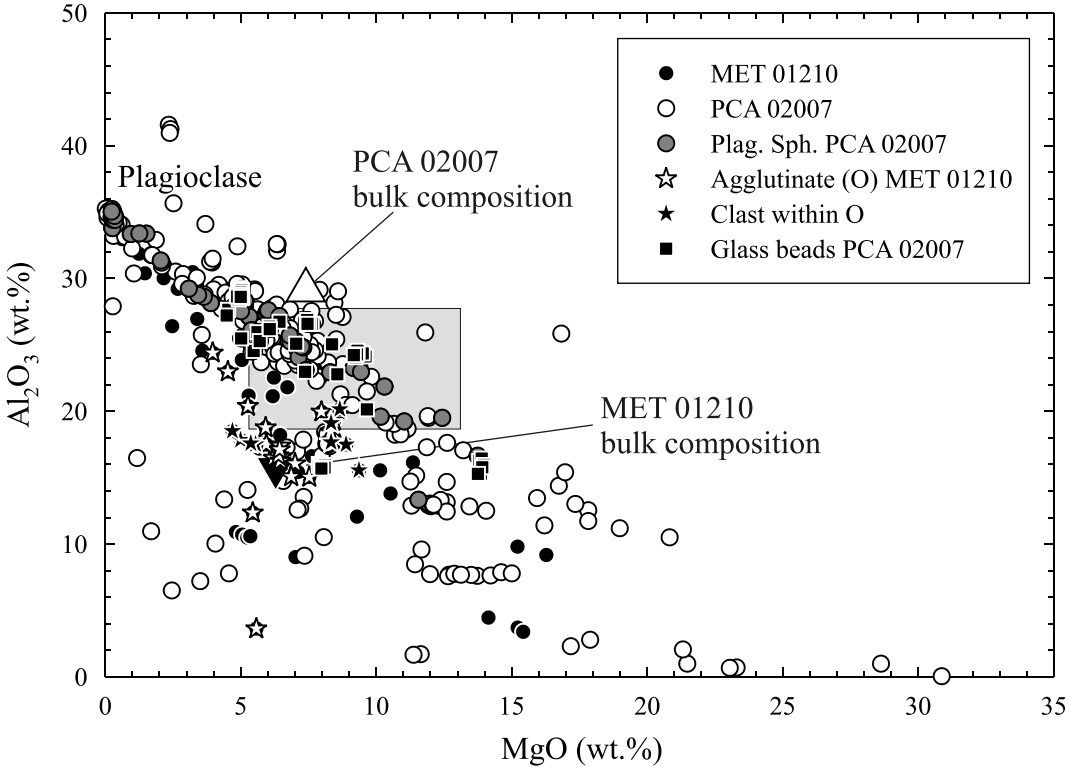

Fig. 5. Compositions of glasses in PCA 02007 and MET 01210 according to type (Al-rich spherule, agglutinate, glass beads) plotted on an MgO versus Al_2O_3 discrimination diagram. Also plotted are whole-rock compositions for MET 01210 (filled triangle) and PCA 02007 (unfilled triangle) and the approximate range of glass compositions in ALHA 81005, MAC 88105 and Apollo 16 regolith (Grey box—Delano, 1991): a larger range of glass compositions, trending to more aluminum-rich compositions, have been observed in other Apollo 16 regolith materials (R. Zeigler pers. comm.). The composition of the agglutinate fragment in MET 01210 is less Al_2O_3-rich than PCA 02007 agglutinates, but all indicate mixing with a plagioclase-rich end-member. Glass bead compositions in PCA 02007 are generally homogeneous but trend to high Al_2O_3 indicating that the majority (all?) of these glass beads have an impact, not volcanic, origin. Glasses with low MgO and low Al_2O_3 in PCA 02007 are generally rich in FeO and have up to 3 wt% TiO_2, perhaps reflecting an ilmenite component.

(<20 μm) rounded mineralic clasts, but the most predominant olivine clasts have low forsterite contents like those found within the lithic basalt clast lithologies (e.g., A and AA). A peculiarity of MET 01210 is the presence of large clasts of fayalite (⩾500 μm) which are associated with ilmenite, but lack inclusions of K-glass and silica like those seen in many lunar basalt mesostases (e.g., Dhofar 287 or LAP 02205; Anand et al., 2003, 2006). A similar mineral association is seen in Clast A where the largest fayalites are not associated with the mesostasis and appear to have crystallized concomitantly with ulvöspinel.

Other mineral fragments and matrix constituents within MET 01210 include plagioclase (up to 2 mm in length; $An_{98–68}$; Fig. 2d), ilmenite (bladed, up to 0.8 mm; 0.85–<0.1 wt% MgO) and Al_2O_3-rich to Al_2O_3-poor glass (Fig. 5). Glasses analyzed include fusion crust and agglutinates—no spheroids or silica-poor glasses were recognized, although some have been reported for MET 01210 in preliminary petrographic studies (Zeigler et al., 2005a; Huber and Warren, 2005). Spinels (up to 0.8 mm in length) contain less than 10 wt% Cr_2O_3 and are ulvöspinels (Fig. 6). Ulvöspinels are also the most common spinels in the basalt clasts and are found associated with late-stage Fe-rich pyroxene or associated with ilmenite or fayalite. A single spinel has a chromite core (38.8 wt% Cr_2O_3, 7.6 wt% TiO_2) zoned to an ulvöspinel rim (13.9 wt% Cr_2O_3, 25 wt% TiO_2; Fig. 6).

Minor phases include apatite (up to 50 μm on the longest axis, 1.7–2.2 wt% F, 1.7–2.0 wt% Cl) and merrillite (4.6 wt% Ce_2O_3), as well as silica, troilite and FeNi metal grains. Silica occurs as grains up to 0.4 mm in diameter and is >99 wt% SiO_2. Troilite is located within lithic clasts (Table 2) and within the matrix. FeNi metals occur as <20 μm grains throughout the matrix. Three high Co, low Ni metal grains, similar to those described in LaPaz and Apollo 12 mare basalts (Day et al., 2006) were recognized, although the majority of grains have low Co, with a distinct group possessing elevated (>0.25 wt%; Fig. 7) P, indicative of an exogenous (meteoritic) component in MET 01210. The matrix is well consolidated and partially welded by irregular agglutinate fragments and small mineral clasts, with compositions identical to the mineral clasts and lithic fragments described.

3.2. Petrography and mineral chemistry of PCA 02007

Pecora Escarpment (PCA) 02007 is a 22.4 g feldspathic regolith breccia discovered in Antarctica in 2003 (Fig. 8a–p).

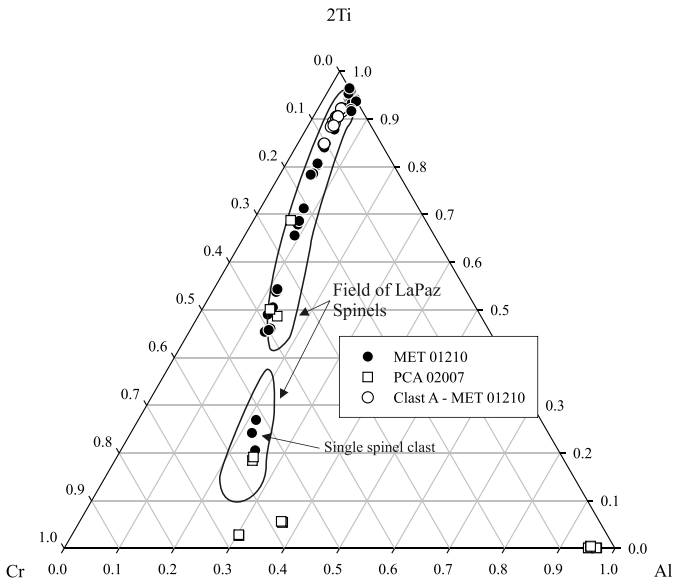

Fig. 6. 2Ti–Cr–Al plot for PCA 02007 and MET 01210 spinels, which show a typical low-Ti mare basalt fractionation trend. Note the nearly pure spinel measured in PCA 02007. Fields are for spinels from the LaPaz evolved low-Ti lunar mare basalt meteorites (Day et al., 2006).

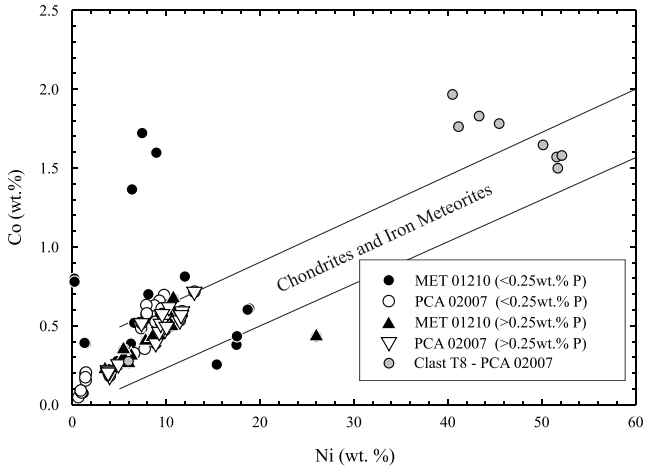

Fig. 7. Ni versus Co for FeNi metal grains in PCA 02007 and MET 01210 and for meteorite clast T8 in PCA 02007. PCA 02007, Clast T8 and MET 01210 contain FeNi metal grains with similar Ni/Co ratios to chondritic meteorites (data from Goldstein and Yakowitz, 1971), including some FeNi metal grains with elevated P contents.

Using the terminology of Stöffler et al. (1980), PCA 02007 can be considered a mature, polymict, predominantly feldspathic regolith breccia. It is texturally and petrographically similar to previously described feldspathic lunar meteorites (e.g., Korotev et al., 2003) and is composed of individual lithic clasts (Tables 1 and 2) and mineral fragments set within a fine-grained, partially glassy matrix. It is worth noting that all feldspathic lunar meteorites are breccias. Plagioclase-rich metamorphic clasts from an anorthositic precursor, dominate the clast assemblage in PCA 02007 (Fig. 8). Basaltic, noritic, troctolitic, granulitic, agglutinitic and partially devitrified spherule clasts are also present (Fig. 8b–h). A distinct and unique 'chondrule-like' clast located within PCA 02007,24, and first reported by Taylor et al. (2004b), is described in detail here (Fig. 8a). Individual minerals within the breccia in decreasing order of abundance are plagioclase, pyroxene, olivine, spinel, ilmenite, troilite and FeNi metal grains (Table 7).

3.2.1. Feldspathic clasts

There are a variety of textures for the feldspathic clasts in PCA 02007, all of which have been melted or recrystallized and can thus be considered meta-anorthosites or feldspar-phyric metamorphic clasts (Fig. 8m–p). Some clasts have a poikilitic texture of small olivine, pyroxene and FeNi metal grains that are enclosed by plagioclase (e.g., clast T2, Fig. 8h). A large proportion of feldspathic clasts have recrystallized subophitic to hyaloophitic textures (e.g., Fig. 8m–p), often with bladed or dendritic plagioclase crystals and vermicular FeNi metal grains. Large FeNi metal grains often occur as large (>20 μm) bright hued spots in BSE images (e.g., Fig. 8f). Like FeNi metals in feldspathic clasts of MET 01210, these are almost certainly exogenous (meteoritic) in origin. There is also a subset of 'comb-textured clasts' of plagioclase and Mg–Fe rich glass (Fig. 8m), and partially resorbed and melted crystals (olivine, pyroxene, plagioclase) enclosed within recrystallized material (e.g., Fig. 8p).

The metamorphic feldspathic clasts typically have plagioclase with high anorthite contents ($\sim An_{94-98}$) and accessory pyroxene and olivine compositions that span the range of compositions from ferroan anorthosites to high magnesium (high Mg/Fe) suite rocks (e.g., Table 2). These clasts usually contain FeNi metal grains that either have high phosphate abundances or lie within the range of chondrite and achondrite meteorite compositions (Fig. 7; Section 3.2.5). One distinct poikilitic textured feldspathic clast (T2) partially overlaps the compositions of sodic anorthosites recognized by Norman et al. (1991). Another clast contains olivine (Fo_{86}) that is clearly more Mg-rich than the co-existing pyroxenes, indicating mineralogical disequilibrium (clast W, Table 2).

3.2.2. Basalt/gabbro igneous and metamorphic basalt clasts

Because of the predominance of feldspathic metamorphic clasts, it is not surprising that PCA 02007 has a population distribution of plagioclase that trends to high anorthite contents and a pyroxene population that has a predominance of orthopyroxene, pigeonite and augite compositions (Fig. 9a–d). There is, however, an obvious tail to lower anorthite contents for plagioclase and a large range in pyroxene compositions to pyroxferroite, which reflects the contribution of basaltic and metamorphic basaltic fragments in PCA 02007. Basaltic clasts in PCA 02007 generally have more magnesium olivine and pyroxene compositions than basaltic fragments recognized in basaltic breccia meteorites like MET 01210,

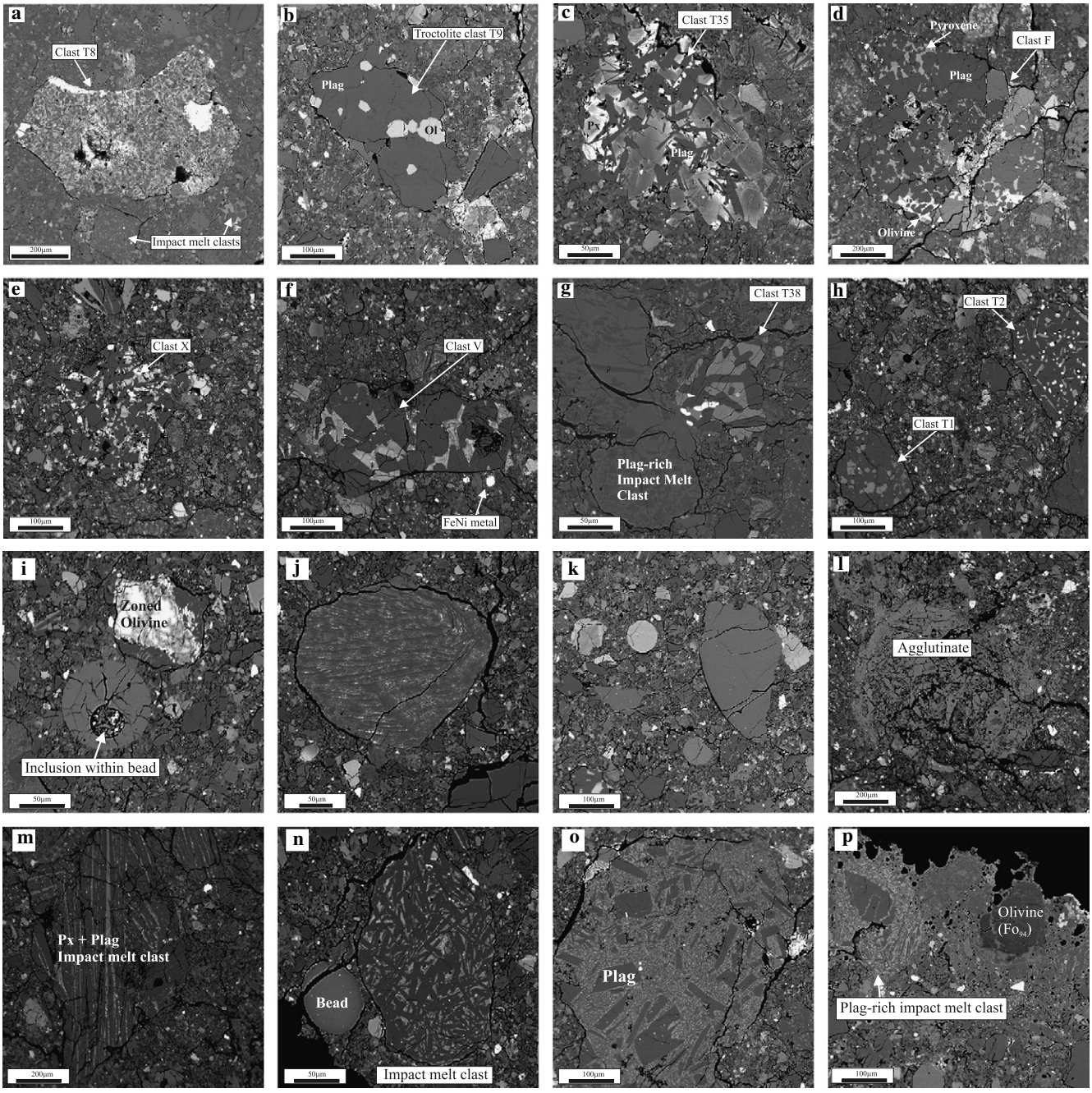

Fig. 8. BSE images of textural features and clast types in PCA 02007. (a) 'Chondrule-like' clast, T8, showing zones of pyrrhotite (brightest), porphyritic olivine (dark grey) and interstitial plagioclase and glass (medium grey) that make up this highly unusual included fragment in PCA 02007. Close to this clast are a number of plagioclase-rich impact melt clasts. (b) Poikilitic troctolite clast (T9) composed of plagioclase with high anorthite contents (dark grey) and olivine. (c) Sub-ophitic annealed impact melt basalt clast (T35) with acicular plagioclase crystals (dark grey) set within zoned pyroxene. (d) Ophitic basalt/gabbroic clast (F) with blocky plagioclase (dark grey) set within pyroxene (top of clast) and olivine (bottom of clast). (e) Poikilitic basaltic impact melt clast (X) with ilmenite (bright hue), pyroxene and plagioclase (dark hue). (f) Subophitic norite clast (V) composed of large euhedral to subhedral plagioclase and pyroxene. (g) Basalt clast (T38) next to a plagioclase-rich impact melt clast. Note the rounded edges of the ilmenite and plagioclase in clast T38. (h) Clasts T1 and T2 in PCA 02007 illustrating the variety of compositional clasts and textures. Glassy or partially melted impact melt clasts are common in PCA 02007, and range from rounded spherules with included minerals (i), fast-quenched spherules with 'comb-like' plagioclase and/or pyroxene growths (j), chemically homogenous low-Ti spherules, often with high Al_2O_3, and rounded or disaggregated types (k), or agglutinates (l). The lithic clast population of PCA 02007 is dominated by impact-melt and metamorphic textures with comb-like plagioclase-pyroxene intergrowths (m), re-annealed feldspathic clasts (n, o) and impact melt clasts containing partially resorbed minerals (e.g., olivine and plagioclase) (p).

although some possess a range of pyroxene compositions that follow a 'Fenner' Fe-enrichment trend (e.g., clast T35; Table 2, Fig. 9). Based on the wide range of textures (e.g., Fig. 8c–g) and chemical compositions a number of different basaltic clast populations can be recognized in PCA 02007, that are described here.

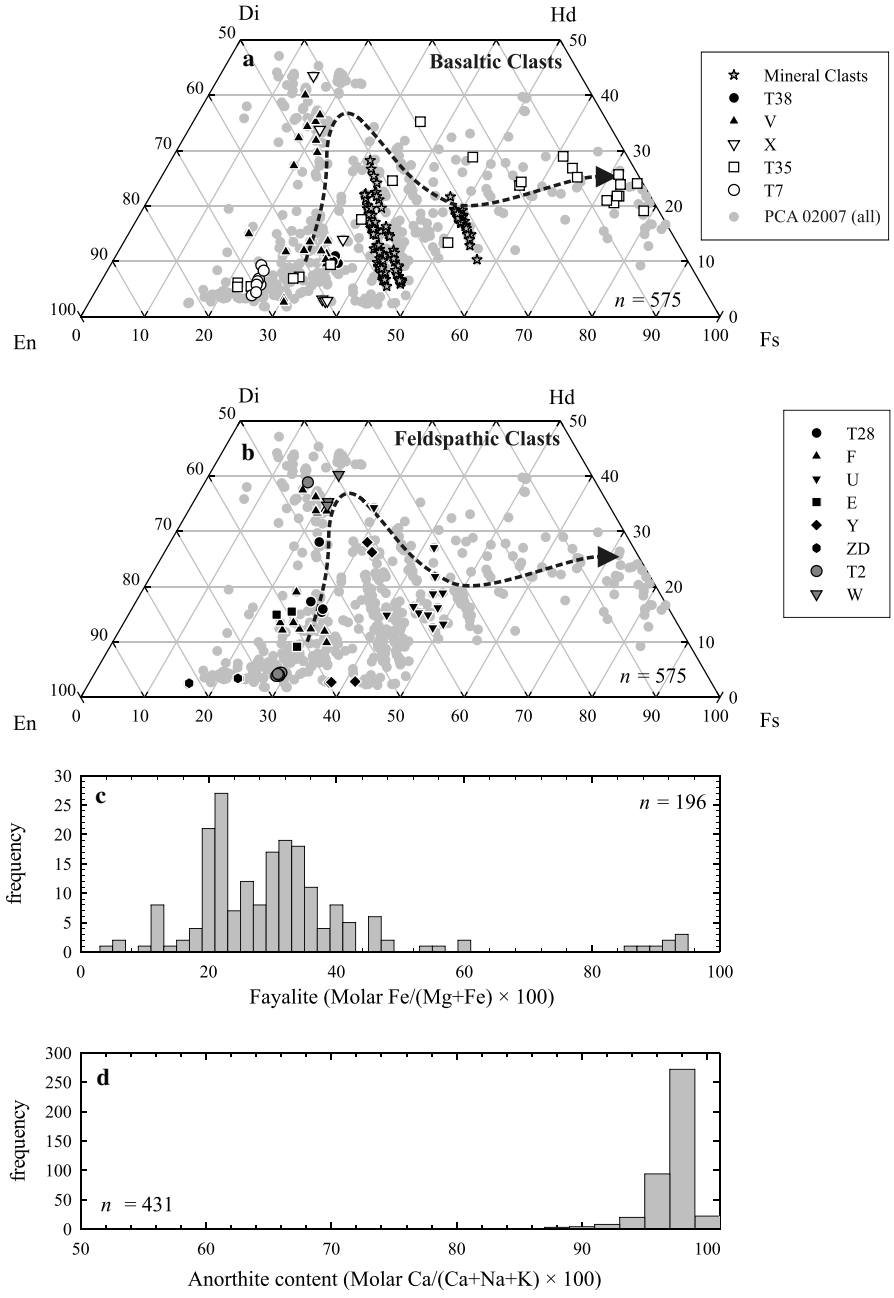

Fig. 9. Pyroxene, olivine and plagioclase compositions for selected lithic and mineral clasts in PCA 02007. Grey shaded circles in (a and b) are data points obtained on all pyroxenes in PCA 02007 during the course of this study. Pyroxene quadrilateral for basaltic (a) and feldspathic (b) lithic clasts and mineral clasts. Compositions of pyroxenes in the basaltic clasts (e.g., T35) cover nearly the entire range of pyroxene compositions measured in PCA 02007, similar to some basaltic clasts in MET 01210. However, the core compositions of these basaltic clasts are generally more Mg- or Ca-rich than core compositions of typical mare basalt pyroxenes. Compositions of pyroxenes are compared with zoning trends in pyroxenes from experiments on lunar basalt 15597 (dashed, arrowed line—Grove and Bence, 1977). There is overall, a very wide range in pyroxene compositions measured in PCA 02007, although feldspathic clasts do not possess Fe-rich pyroxenes. Pyroxene clasts with exsolution lamellae show a range of pyroxene compositions, as shown in (a). (c) Olivine compositions for PCA 02007 illustrating the preponderance of forsteritic olivines in the sample; fayalitic olivines are restricted to basalt clasts (olivine and plagioclase in clast T8 have been omitted from this plot for clarity). (d) Plagioclase compositions for PCA 01210, showing fewer low anorthite compositions compared with MET 01210 (Fig. 2d).

Basaltic clasts can be divided into subophitic and re-annealed, metamorphic, pilotaxitic to poikilitic varieties (e.g., Fig. 8c and e; Table 2). For the purpose of this study, the distinction between ophitic basalt and gabbro clasts has been made based on their average plagioclase lengths ($\leqslant$50 μm for 'basalts'; U and T38; Fig. 8g, and $\geqslant$200 μm for the 'gabbros'; T28 and F; Fig. 8f). The ophitic basalts and gabbros have olivine with $Fo_{55–65}$, plagioclase compositions that vary from $An_{90–98}$ and a range of pyroxene compositions (Fig. 9a and b). Ti/Al ratios for basalts clasts in PCA 2007 range as a function of the metamorphic or impact-melt heritage of many of the clasts. For crystalline

basalt clasts, Ti/Al ranges from 0.25 to 0.5 consistent with early pyroxene crystallization followed by plagioclase co-crystallization (Fig. 10). Clasts F and T38 contain pyroxenes with a wide range of Ti concentrations for a limited range of Al concentrations and may reflect the relative incompatibility of Ti and Fe in these melts with increasing fractional crystallization.

Metamorphic basalt and gabbroic clasts can be grouped into those with high-Mg pyroxene compositions (E, T7) and those with pyroxene compositions more typical of mare basalts (X, T35; Table 2). These clasts essentially represent crystalline impact melt clasts. High-Mg pyroxene meta-basalts (clasts E, T7) have olivines with $Fo_{64–70}$ and plagioclase from $An_{89–97}$ (Fig. 9). Clasts X and T35 have marginally lower Mg–olivine ($Fo_{52–68}$) and a similar distribution of plagioclase ($An_{87–95}$) and pyroxene compositions (Fig. 9). Pyroxene chemistry for the metamorphic clasts indicates a fast, single stage crystallization history, where pyroxenes generally lie along a single Ti/Al ratio line in Fig. 10 consistent with their impact melt heritage. Clast T35 has pyroxenes with Ti/Al ratios that range from $\leqslant$0.25 to 1. This probably indicates initial saturation in Al and subsequent crystallization of plagioclase and enrichment in Ti in this fast-cooled clast.

3.2.3. Norite, noritic anorthosite and troctolite clasts

Clasts similar to 'high-magnesium suite' type lithologies are relatively abundant in PCA 02007. They have igneous to metamorphic textures, with poikilitic textures

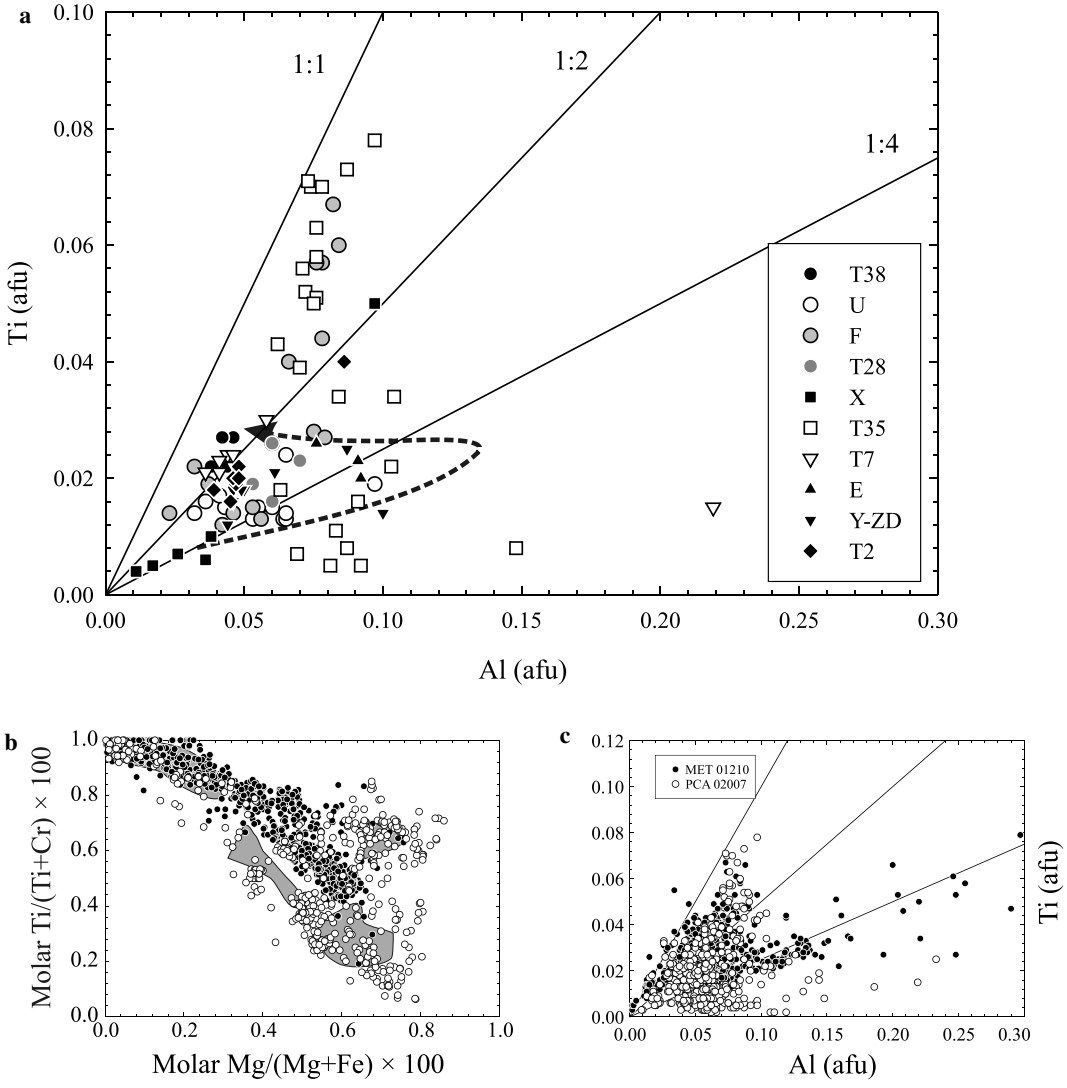

Fig. 10. Pyroxene chemistry for (a) lithic clasts in PCA 02007 as a function of Ti and Al (atomic formula units) and comparison plots (b and c) of pyroxene chemistry for PCA 02007 and MET 01210 as functions of Mg# (Mg/(Mg + Fe) afu) and Ti# (Ti/(Ti + Cr) afu) and Ti and Al (afu). Note that the majority of pyroxenes measured in PCA 02007 are from lithic clasts with a metamorphic or impact melt heritage so the methods of recognizing crystallization sequences (Bence and Papike, 1972) do not necessarily apply. Data are compared with pyroxene crystallization experiments from Grove and Bence (1977—dashed arrowed line) in (a), and with data from EET 96008 (Anand et al., 2003) in (b). PCA 02007 pyroxenes have lower Ti# and higher Mg# than MET 01210 pyroxenes. Lines denoted 1:1, 1:2, 1:4 indicate ratios of Ti/Al = 1, 0.5 and 0.25, respectively.

for troctolites (Fig. 8b, f and h) and ophitic to sub-ophitic textures for norites and noritic anorthosites. Most of the high-magnesium suite-type clasts contain plagioclase with high anorthite contents ($An_{95–98}$). The troctolites contain olivines with restricted ranges in chemical composition for individual clasts, although the two troctolites featured have different forsterite compositions (Table 2). Norites have high-Mg pigeonite (e.g., ZD, Y) and gabbro-norites possess forsteritic olivine (e.g., T2). Despite their metamorphic textures and origins, noritic clasts have pyroxenes with Ti/Al ratios consistent with crystallization from an Al-saturated magma, whereas the gabbro-norite includes pyroxenes with higher Ti/Al ratios, possibly consistent with co-crystallization of plagioclase and pyroxene.

3.2.4. Glass spherules and agglutinates

Numerous glass beads are preserved in PCA 02007. Typically, only the smallest (<150 μm) beads preserve their ideal spherical shape (Fig. 8i–k) whereas the larger beads tend to be fragmented, with their spherical outer edges only partially preserved (Fig. 8k). Nearly all the glass beads in PCA 02007 have magnesium numbers (Mg#) in the range of 61–69, and low TiO_2 (0.2–1.1 wt%) and are chemically homogenous (Table 6). The chemical and textural homogeneity may be consistent with a volcanic origin for some of the glass beads. If they are indeed volcanic, these would be considered very-low titanium (VLT) compositions according to pyroclastic glass classifications (Delano, 1986; Papike et al., 1998). There are obvious textural similarities with the glass beads reported for PCA 02007 (Fig. 5) and those featured in Fig. 30 of Papike et al. (1998). Although some of the glass beads have 'low' Al_2O_3 (15.8 wt%), possibly consistent with a volcanic origin (e.g., Clast T20a, Table 6), the great majority possess very high Al_2O_3 (24–29 wt%) more consistent with an impact melt origin from an anorthositic precursor (Table 6; Fig. 5). One glass bead (26.7 wt% Al_2O_3) contains a small (30 × 25 μm) included pocket of crystals (olivine, pyroxene and plagioclase) and glass (Clast T3, Table 6; Fig. 8i). The olivine has a high Mg-number (Fo_{80}) and the plagioclase is calcic (An_{95}). This pocket of crystals and glass may represent the crystallization products of the impact melt that produced the glass bead.

Agglutinate clasts commonly occur as broken fragments or as spherical clasts with vesicles, schlieren and inhomogeneous textures (Fig. 8l). Agglutinate clasts with homogeneous glass compositions (e.g., Clast T13; Table 6) can be distinguished from the volcanic glass beads because of the abundance of vesicles and sub-micrometer Fe^0 particles. The agglutinates are chemically heterogeneous. For example, one agglutinate has MgO ranging from 0.1 to 30 wt% and Al_2O_3 from 0.1 to 35 wt%. Such variability is most likely a function of the incomplete mixing and break-down of ferromagnesian minerals and plagioclase that are disaggregated and melted to form agglutinates.

3.2.5. Chondrule-like clast in PCA 02007

A ~0.6 × 0.4 mm fragment of a chondrule-like object occurs within PCA 02007 and has been designated clast T8 (Tables 1 and 2; Fig. 8a and 11). Texturally the clast is porphyritic, dominated by equant olivines (46.5 vol %) set within a matrix rich in glass (28.8 vol %) and plagioclase (19.9 vol %) (Fig. 11). The clast also contains pockets of sulphide and FeNi metal (4.8 vol %; Table 1). Differences between this clast and typical chondrules include the angular and fragmented nature of the silicate minerals and the absence of pyroxene. It contains highly forsteritic olivine cores with high CaO and Cr_2O_3 contents, nearly chondritic

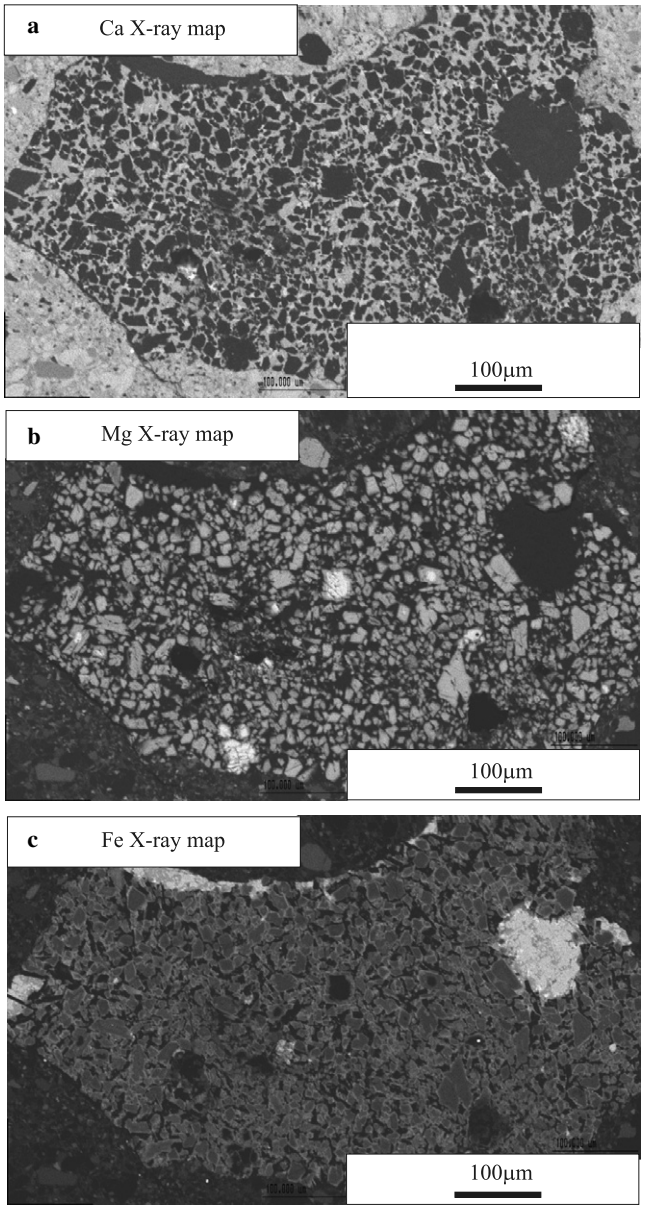

Fig. 11. Ca (a), Mg (b) and Fe (c) X-ray maps of clast T8 in PCA 02007 illustrating the (a) Al-rich nature of the matrix surrounding the olivine, (b) the few highly forsteritic olivines in the clast, and (c) the zonation of the olivine grains with respect to Fe as well as pentlandite and pyrrhotite assemblages (bleb-like bright hued regions).

REE patterns, and Fe/Mn ratios (11 ± 8), which are unlike any lunar material investigated to date.

A number of the olivine cores in clast T8 are highly magnesian (Fo_{99}) with rims that range from Fo_{82} to as Fe-rich as Fo_{44} (rims have a maximum width of <10 μm and an average width = ~2 μm). The core-to-rim variations result in a bi-modal distribution of forsterite contents (Fig. 12a). Cr_2O_3 contents for olivines (Fig. 12b) lie between the range of compositions for chondrules found in CV and CR chondrites (Krot and Keil, 2002a; Krot et al., 2002b), but the anorthite and MgO content of plagioclase ($An_{80\pm1}$; MgO = 0.27 ± 0.09 wt%) best fit the compositional range

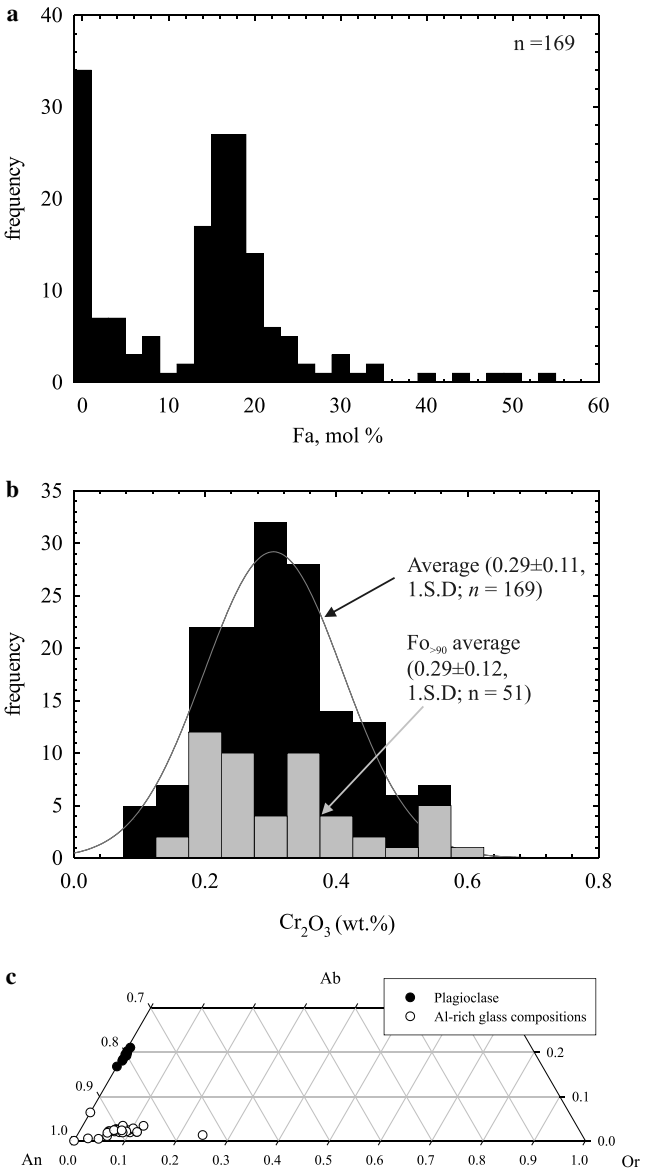

Fig. 12. Olivine (a, b), plagioclase and glass (c) compositions for clast T8 in PCA 02007. Note the bimodal distribution of olivine compositions at ~Fo_{100} and ~Fo_{80} as well as the tail to fayalitic olivine compositions. Also shown in (b) are the average Cr_2O_3 contents for undifferentiated olivines versus olivines with $Fo_{>90}$ illustrating the similarities in averages and the broad Gaussian distribution.

of CV plagioclase-rich chondrules, if this clast is, indeed, of a chondritic heritage. The glass in the meteorite clast has a high FeO content (Table 8) and is compositionally homogeneous, apart from specks of <1 μm Cr-rich material (possible chromite grains) recognized from X-ray mapping of the clast. FeNi metal containing ~6 wt% Ni occurs within olivine clasts. More commonly, FeNi metal occurs with the sulphides and has 40–52 wt% Ni, P_2O_5 below the detection limit of analysis (<0.03 wt%), and chondritic Co/Ni ratios (~0.048; Fig. 7). The sulphide assemblage consists of pyrrhotite with up to 4.8 wt% Ni and pentlandite with up to 0.6 wt% Co and 0.2 wt% Cu. Such an assemblage is typical of Fe–Ni–S monosulphide solution that underwent exsolution during cooling. It should be noted that the presence of pyrrhotite and pentlandite in pristine lunar rocks has never been documented.

The reconstructed major element composition of clast T8 (Table 9) yields Mg/Si and Fe/Si ratios similar to chondrites, with CaO contents that are low. These low refractory element contents preclude significant mixing with lunar materials. Incompatible element concentrations of individual silicate mineral phases for the chondrule clast are presented in Table 8 and REE patterns are shown in Fig. 13. The REE patterns are variable with abundances that range from ~0.5 × CI to ~13 × CI, with Mg-rich olivines having the lowest and glass having the highest REE concentrations, with plagioclase intermediate between the two. Plagioclase grains have positive Eu anomalies, however, none of the other minerals and glass have the characteristic Eu anomalies typical to most lunar minerals (e.g., Fig. 4). Positive Eu anomalies are not unusual for chondritic feldspars (Brearley and Jones, 1998). The reconstructed whole-rock REE pattern is ~7 × CI chondrite for the LREE and ~4 × CI for the HREE (Fig. 13).

3.2.6. Mineral clasts and matrix

The predominant mineral clast in PCA 02007 is plagioclase, which has a similar compositional range as those found in lithic clasts (An_{95-99}; Table 7, Fig. 9d). These occur in a wide variety of forms from anhedral masses, to individual clasts. The high anorthite component of the plagioclase is typical of feldspathic regolith breccias (e.g., Takeda et al., 1992; Arai and Warren, 1999; Anand et al., 2003). Low anorthite contents (An_{70-82}) were measured in a single grain, which also contained silica indicating fractionation of the parental melt for this clast, which may be a fragment of basaltic material.

Pyroxene occurs within PCA 02007 mainly as individual clasts that account for the large range of compositions observed in Fig. 9. Ferropyroxene compositions were measured in five mineralic clasts (50–100 μm in diameter) and some of the most Ca- and Mg-rich pyroxene compositions were measured in suspected non-mare clasts. Probe traverses across a number of individual pyroxene grains revealed exsolution lamellae, which were also noted from optical observations. The width of the exsolution lamellae average

Table 9
Whole-rock major and trace element compositions for MET 01210 and PCA 02007

Sample	MET 01210					PCA 02007		
Method	EMP FC		EMP FC[a]	Clast A Modal[d]	Clast AA Modal[d]	ICP WR	EMP FB[b]	Clast T8 Modal[d]
wt%		*St. Dev.*						
SiO_2	44.8	*0.48*	44.8	46.9	44.9	*38.6*[c]	44.6	40.7
TiO_2	1.64	*0.06*	1.58	1.76	0.20	0.28	0.28	0.40
Al_2O_3	16.2	*0.19*	17.0	12.7	26.0	29.1	26.4	8.68
Cr_2O_3	0.17	*0.04*	0.19	0.38	0.03	—	0.16	0.16
FeO	16.9	*0.52*	16.2	17.0	9.67	6.80	6.26	16.4
MnO	0.24	*0.06*	0.26	0.31	0.13	0.09	0.09	0.18
MgO	6.50	*0.14*	5.97	6.13	1.51	7.40	6.70	21.7
CaO	13.0	*0.16*	13.6	14.3	16.7	17.3	15.3	8.63
Na_2O	0.28	*0.03*	0.26	0.35	0.39	0.38	0.33	0.67
K_2O	0.06	*0.02*	—	0.05	0.02	0.05	0.02	0.12
P_2O_5	0.24	*0.04*	—	0.08	—	0.08	0.03	0.35
SO_2	—	—	—	—	—	—	—	1.99
Total	100.0	$n = 22$	99.9	100.0	99.6	61.4	100.2	100.0
Mg#	40.8		39.6	39.2	21.8	66.0	65.6	70.2
p.p.m								
Li	—		—	—	—	4.23	—	—
Be	—		—	—	—	0.44	—	—
Sc	—		—	53	222	7.95	—	15
V	—		—	73	32	48.2	—	72
Cr	—		—	1906	1303	656	—	—
Co	—		—	—	—	23.0	—	—
Ni	—		—	—	—	292	—	—
Cu	—		—	—	—	4.77	—	—
Zn	—		—	—	—	10.9	—	—
Ga	—		—	—	—	2.33	—	—
Rb	—		—	—	—	0.56	—	3.1
Sr	—		—	143	16	140	—	44
Y	—		—	5.5	37	8.23	—	5.3
Zr	—		—	3.5	36	32.2	—	16
Nb	—		—	—	—	2.55	—	—
Cs	—		—	—	—	0.06	—	—
Ba	—		—	21	0.2	33.4	—	8.5
La	—		—	14	0.6	2.49	—	1.4
Ce	—		—	37	2.7	7.11	—	2.6
Pr	—		—	5.0	0.6	0.97	—	0.4
Nd	—		—	22	4.4	4.78	—	1.8
Sm	—		—	5.0	1.9	1.56	—	0.5
Eu	—		—	1.4	0.2	0.77	—	0.3
Gd	—		—	6.0	3.4	1.79	—	0.6
Tb	—		—	1.1	0.7	0.36	—	0.1
Dy	—		—	6.5	5.7	1.86	—	0.8
Ho	—		—	1.2	1.0	0.40	—	0.2
Er	—		—	2.9	3.5	1.04	—	0.5
Tm	—		—	0.3	0.5	0.15	—	0.1
Yb	—		—	1.5	3.1	1.07	—	0.5
Lu	—		—	0.1	0.5	0.15	—	0.1
Hf	—		—	—	—	1.07	—	—
Ta	—		—	—	—	0.21	—	—
W	—		—	—	—	0.00	—	—
Pb	—		—	—	—	0.71	—	—
Th	—		—	—	—	0.47	—	—
U	—		—	—	—	0.14	—	—

Abbreviations: EMP FC/FB = Electron Microprobe Analysis of Fusion Crust/Fused Bead; ICP WR = Inductively Coupled Optical Emission Spectrometry (major elements) and PQII (trace elements) of whole-rock.
The italic font indicates the standard deviation data for the whole rock major-element analyses.
[a] Zeigler et al. (2005a).
[b] Zeigler et al. (2004).
[c] SiO_2 in PCA 02007 ICP WR calculated by difference.
[d] Modal recombination from average mineral compositions and modal abundance data (Table 1). This technique is susceptible to the presence of accessory phases (e.g., merrillite, zirconium-rich minerals) with elevated minor element abundances and to the surface area versus grain size effect (see text).

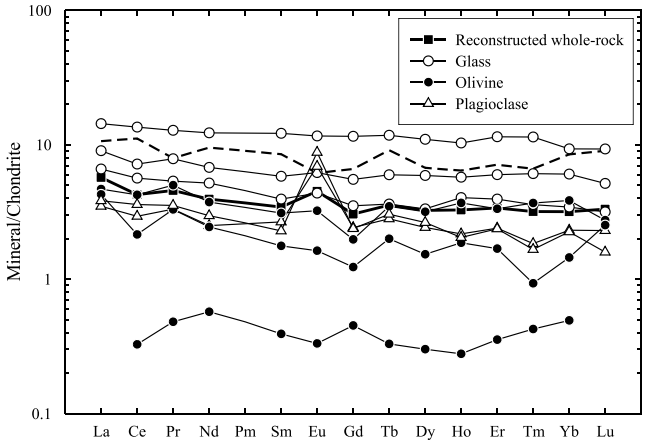

Fig. 13. CI chondrite-normalized REE abundances in clast T8 of PCA 02007. Minerals and glass have nearly flat REE patterns. The glass has the highest abundances of REE and plagioclases have positive Eu anomalies. The whole-rock recombination is based on the modal abundance and average composition of mineral and glass phases in clast T8. The dashed line indicates the composition of glass in typical ordinary chondrules (Alexander, 1994). Normalization data from Anders and Grevesse (1989).

2.1 ± 0.6 μm, similar to those seen in MET 01210. Olivine mostly occurs within clasts of basalt or troctolite (Fig. 8b and d). Forsterite contents range from Fo_{80} to Fo_5, although there are some olivine clasts with very high forsterite contents (up to Fo_{94}).

Minor mineral clast constituents of PCA 02007 include spinel, ilmenite, FeNi metal, troilite and silica. Spinels are rare in PCA 02007, although both Al-rich chromite and ulvöspinel were analyzed (Fig. 6). A single spinel clast was found to be almost stoichiometrically pure spinel ($[Mg_{0.9}Fe_{0.1}][Al_{1.9}]O_4$). Ilmenites are rare outside of the basaltic clasts. The ilmenites that do occur as individual clasts have low MgO contents, with only one ilmenite clast possessing high MgO (4.7 wt%). There is an abundance of FeNi metal grains in PCA 02007 in the size range of 1–50 μm, and they have low Co contents for a given Ni composition, indicating a meteoritic origin for these metals. High P_2O_5 metal grains occur as discrete clasts or within anorthositic melt clasts and generally have slightly higher Co contents than low P_2O_5 metal grains (Fig. 7). Troilite and nearly pure silica clasts (>98 wt% SiO_2) occur in the matrix but no phosphate minerals were recognized. The remaining matrix of PCA 02007 is made up of a sintered mass of lithic and mineral clasts and glass with compositions identical to the mineral clasts and lithic fragments described.

3.3. Bulk compositions of MET 01210 and PCA 02007

Major element concentrations were estimated by modal recombination of clasts A and AA (MET 01210) and the meteorite clast T8 (PCA 02007), by measurement of the fusion crust for MET 01210, and by analysis of whole-rock powder for PCA 02007 (Table 9). The method of modal recombination employed is identical to that of Fagan et al. (2003), who noted the pit-falls of unrepresentative sampling, but assessed the major oxide concentrations to have around 10% relative error. Major element compositions for other clasts (Table 1) are not presented because of their generally small sizes proportional to their grain size, which could result in unrepresentative calculated compositions. Both MET 01210 and clast A and AA represent low TiO_2 basalts, with the Mg-number for the breccia whole-rock being slightly higher than, but similar to that of clast A. MET 01210 is dissimilar to other basaltic or mixed (basaltic-feldspathic) breccia meteorites, having generally higher FeO and lower MgO than mixed breccias, and higher Al_2O_3, lower TiO_2 and FeO than most basaltic lunar meteorites (Fig. 14). This variation in chemistry is a direct function of the large proportion of evolved and Fe-rich basaltic material and plagioclase within MET 01210. Trace element compositions for clast A and AA of MET 01210 have been estimated from modal recombination of mineral phases (Fig. 4d). The REE patterns of these clasts are strongly controlled by phosphates (especially merrillite) in modal recombinations and indicate significant LREE-enrichment in these clasts with much steeper REE patterns than for mare basalt meteorites.

PCA 02007 has a similar whole-rock composition to feldspathic regolith breccia meteorites ALHA 81005 and Y-791197, with low TiO_2 and Al_2O_3 and high MgO relative to other feldspathic-rich lunar meteorites (Fig. 14). The high Al_2O_3, low FeO and low Th (0.47 ppm) abundances for PCA 02007 are consistent with other feldspathic lunar meteorites, whose whole-rock chemical compositions have been used to generate a new estimate for the Al_2O_3 content of the upper lunar crust (Korotev et al., 2003). REE contents for PCA 02007 are $\sim 10 \times$ CI with a moderately light rare earth element-rich REE pattern and a positive Eu anomaly, features similar to most feldspathic lunar meteorites (Fig. 4d). PCA 02007 also appears to have more elevated REE abundances than most feldspathic meteorites and, in this respect is most similar to feldspathic lunar meteorites QUE 93069 or Dhofar 025/026 (Korotev et al., 2003).

4. Discussion

The discovery, detailed description, and comparison of lunar meteorites with samples from the Apollo and Luna collections, and with other lunar meteorites, is important for understanding lunar remote sensing data (e.g., Korotev et al., 2003) and the geochemical evolution of the Moon (e.g., Warren, 2003; Korotev, 2005). In this discussion we first consider the evidence for lunar origins of brecciated meteorites MET 01210 and PCA 02007. Detailed analyses of basalt clasts A and AA in MET 01210 and clast T8 in PCA 02007 allow us to then compare and contrast these components with known mare basalts and with 'chondrule-like' and chondrule silicate materials,

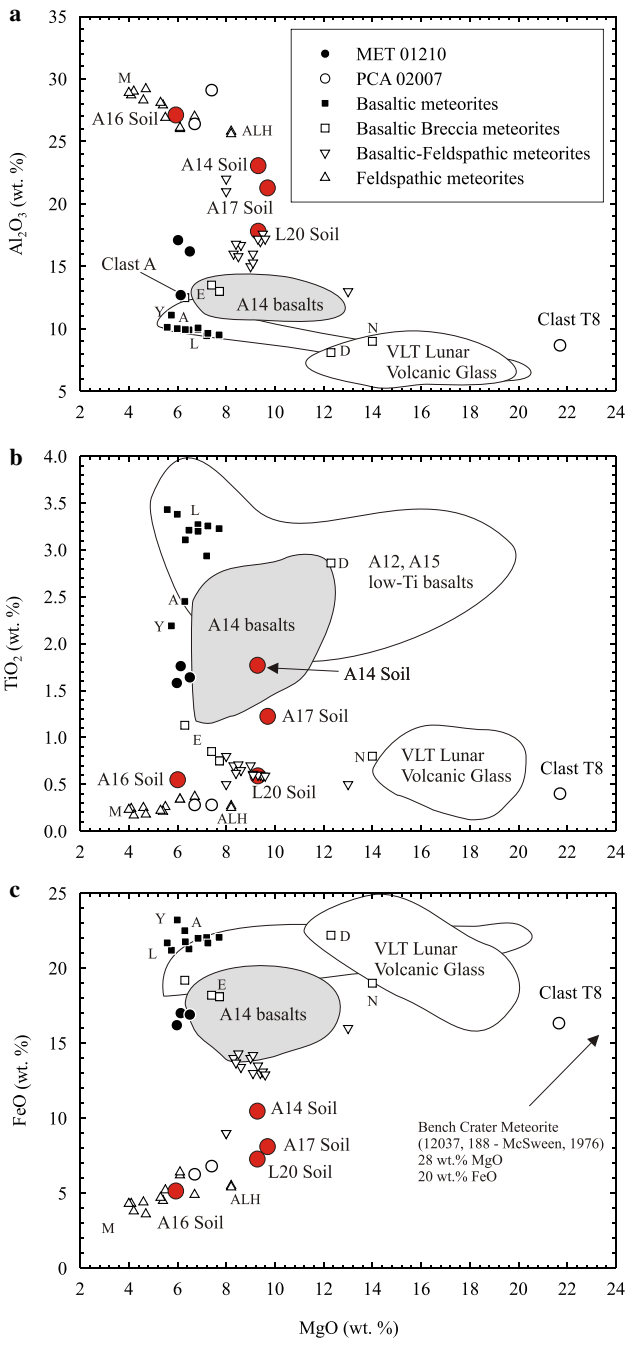

Fig. 14. Whole-rock MgO versus (a) Al_2O_3, (b) TiO_2 and (c) FeO for lunar meteorites (points) and for Apollo samples (fields) and average lunar soil compositions (Warren and Kallemeyn, 1991). Predominantly basaltic meteorite MET 01210 has similar MgO to mare basalts and other basaltic breccias. Feldspathic meteorite PCA 02007 plots at the high MgO range of previously discovered lunar feldspathic meteorite breccias. Clast T8 clearly has an anusual heritage compared with all lunar material described so far. The basaltic meteorites included in the plot are Y-793169 (Y), A-881757 (A), NWA 032, LAP 02205/02224/02226/02436 and LAP 03632 (L). Basaltic breccias include EET 87521/96008 (E), NWA 773 (N) and Dho 287 (D). Mixed feldspathic/basaltic breccias are QUE 94281, Y-793274, Calcalong Creek and Y-983885. Feldspathic lunar meteorites include ALH 81005 (ALH), Y-791197, Y-82192/86032, MAC 88104/88105 (M), QUE 93069, DaG 262/400/025, and NWA 482. Data sources are Korotev (2005), Day et al. (2006) and references therein.

respectively. Finally, we compare MET 01210 and PCA 02007 with previously described lunar breccias and consider the ramifications these meteorites may have for lunar geology.

4.1. Lunar origins for breccia meteorites MET 01210 and PCA 02007

Basalt clasts in both meteorites indicate that they originated from a differentiated planetary body and the presence of vesiculated agglutinate fragments in both meteorites suggests that this parent body lacked an atmosphere. Fe/Mn ratios in pyroxenes (Fe/Mn = 60 ± 8, 1 SD) and olivines (Fe/Mn = 86 ± 9, 1 SD) in MET 01210 are similar to those in PCA 02007 (pyroxene Fe/Mn = 58 ± 8, 1 SD; olivine Fe/Mn = 92 ± 12, 1 SD), with both possessing lower Mn for a given Fe content, than pyroxene (Fe/Mn = ~45) and olivine (Fe/Mn = ~75) in typical unfractionated terrestrial basalts (Fig. 15). This distinct mineral chemical signature is considered characteristic of a lunar origin (Fe/Mn in pyroxene = ~79 and in olivine ~105; Papike et al., 1998) because Fe/Mn ratios appear to be unique indicators of planetary bodies (Dymek et al., 1976; Drake et al., 1989). For the meteorite fragment T8 in PCA 01210, the forsterite cores (>Fo_{95}; and where Mn and Fe are both above detection limits) have Fe/Mn ratios uncharacteristic of lunar rocks (Fe/Mn = 11 ± 8, 1 SD) and more similar to chondrule Fe/Mn ratios (e.g., Papike, 1998), whereas olivine rims with <Fo_{95} have higher Fe/Mn ratios (Fe/Mn = 96 ± 23, 1 SD). Distinct trends can be discerned in molar Mg/(Mg + Fe) versus Fe/Mn space for olivines in clast T8 illustrating that the olivines with the lowest forsterite contents ($Fo_{<80}$) lie along the lunar fractionation trend, whereas olivines with $Fo_{>80}$ fall along an independent trend (Fig. 15b).

Additional evidence for a lunar origin for MET 01210 and PCA 02007 comes from their textural and mineralogical similarities to Apollo samples and their non-terrestrial chemical characteristics (FeNi metal, anhydrous nature and evidence for low fO_2) that firmly place their origin as breccias derived from the Moon. Although not a unique feature to lunar rocks, the strong negative Eu anomaly in a predominantly basaltic meteorite, MET 01210, and a positive Eu anomaly in predominantly feldspathic regolith breccia PCA 02007 are also consistent with a lunar heritage. The Eu anomalies are consistent with the concept of Eu depletion in the mare basalt source, relative to trivalent REE, due to plagioclase-rich crust formation from an early lunar magma ocean (e.g., Wood et al., 1970; Taylor and Bence, 1975). These signatures provide complementary evidence for the lunar origins of MET 01210 and PCA 02007. The most diagnostic signature of a lunar origin, three-oxygen isotope compositions have, thus far, not been measured for either PCA 02007 or MET 01210.

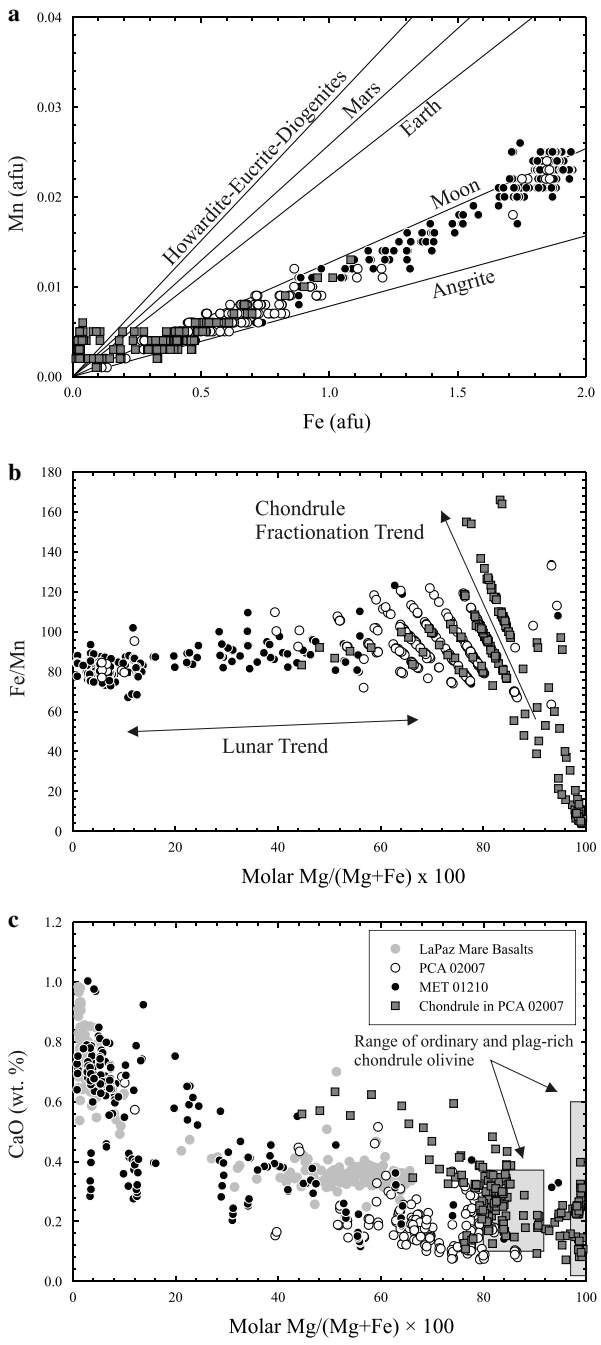

Fig. 15. Plots of (a) Fe versus Mn (in atomic formula units), and (b) molar Mg/(Mg + Fe) versus Fe/Mn and (c) CaO (wt%) for clast T8, versus olivine compositions measured in PCA 02007, MET 01210 and for (c), the LaPaz mare basalt meteorites (from Day et al., 2006). Also shown in (c) are ranges of FeO-rich ordinary chondrule (Jones, 1990) and CV- and CR-type plagioclase-rich chondrules (Krot and Keil, 2002a, Krot et al., 2002b) (Grey boxes). Planetary heritage lines in (a) are from Papike (1998). Fe/Mn ratios for PCA 02007 and MET 01210 support a lunar origin for these meteorites. Olivines in clast T8 are more similar to chondrule olivines than typical lunar olivines, with only the outer few micron rims of the olivines ($Fo_{<80}$) falling along the Fe/Mn versus molar Mg/(Mg + Fe) trend for lunar samples shown in (b); this relationship indicates only minor reworking of the clast with lunar regolith and supports a chondritic heritage for clast T8.

4.2. Basaltic clasts in MET 01210 and comparisons with other low-Ti mare basalts

Although MET 01210 contains evidence for typical regolith components (e.g., agglutinate and feldspathic clasts), it is dominated by highly fractionated basaltic material. This material is clearly of low TiO_2 to very low titanium derivation and has, in mineralogical terms, undergone similar, but more extensive fractionation than the majority of Apollo 12, 14, 15 or Luna 24 low-Ti mare basalt hand specimens (e.g., Brown et al., 1971, 1972; Brett et al., 1971; Coish and Taylor, 1978; Lu et al., 1989). Basaltic precursor material for MET 01210 is also similar to some lunar basaltic meteorites discovered to date (Fig. 14). Studies of the LaPaz mare basalts, NWA 032 and NWA 773 have demonstrated the evolved nature, younger age and likelihood of an incompatible element-rich source, relative to the Apollo 12 and 15 low-Ti mare basalts, for these meteorites (Fagan et al., 2002, 2003; Day et al., 2006). Despite a lack of age constraints and whole-rock trace element data for MET 01210, the basaltic clasts within this meteorite provide important new information on their source regions.

Basalt clasts in MET 01210 have a wide range of textures (Table 2), with fractionated mineral assemblages, including mesostasis and strongly zoned pyroxene, similar to the LaPaz basalts or NWA 032. These textures are igneous and not metamorphic in origin. The basalt clasts also have some geochemical similarities to evolved mare basalts. The most obvious similarities are the core-to-rim variations in pyroxene chemistry resulting in extreme 'Fenner' Fe-enrichment trends from augite through to pyroxferroite (Fig. 2). This iron enrichment is also evident from the abundance of fayalite and ulvöspinel in some of the clasts and is similar to 'Fenner' Fe-enrichment trends documented in Luna 24 basalts (Lu et al., 1989) and in NWA 773 (Fagan et al., 2003). These Fe-enrichment trends may be the result of oxygen fugacity limiting the precipitation of Fe metals or sulphides, enhancing Fe-enrichment in silicates (Snyder et al., 1999). The gross major element and textural similarities that evolved mare basalt meteorites (LAP 02205/02224/02226/02436 and LAP 03632, NWA 032 as well as NWA 773) have with basaltic clasts in MET 01210 may indicate some similarities in terms of their source regions.

Despite similarities with other fractionated mare basalts, the reconstructed REE patterns for the clasts in MET 01210 are strikingly different compared with REE patterns for mare basalts, mare basalt meteorites, or pyroclastic glasses (e.g., Papike et al., 1998). This is due to merrillite subtraction and addition, and the grain size to clast size ratio. This ratio is important because the size of the grains and the surface area of the sample dictate how representative the studied clast is of its precursor material. The HREE-depleted patterns for phosphates in MET 01210 are also unusual and contrast with phosphate REE patterns from previously studied mare basalt meteorites

(e.g., Fig. 4c). Because of the uncertainties of modal analysis on small clasts, and to more accurately compare the clasts with other mare basalts, we have estimated pyroxene equilibrium liquids. If no equilibration of the REE has taken place after crystallization, the equilibrium REE compositions of earliest formed minerals can be used to estimate parental liquid compositions. We compare earliest formed augites (i.e., lowest incompatible element abundances, highest compatible element abundances) from clast A with data from the LaPaz mare basalts (Fig. 16a). Estimated equilibrium compositions using REE partition coefficients for augite (McKay et al., 1986) are plotted as shaded fields in Fig. 16, and illustrate that the equilibrium parental melts for pyroxenes in the LaPaz mare basalts and clast A of MET 01210 are similar. However, the pyroxene equilibrium melts for clast A show no resemblance to its reconstructed whole-rock composition. It is highly unlikely that this disagreement is the result of assimilation and fractional crystallization, or magma mixing processes because plots of enstatite content versus compatible and incompatible elements for pyroxenes do not define mixing trends (Fig. 16b–d). In fact, clasts A and AA have less incompatible element variation within their pyroxenes than LaPaz mare basalts, whose mineralogical compositions have been demonstrated to occur through closed-system crystallization (Anand et al., 2006; Day et al., 2006).

A possible explanation for lack of agreement between modal recombination and pyroxene equilibrium melts are that the phosphate component in clasts A and AA are overestimated for modal recombination, and/or that the phosphates themselves are out of equilibrium with early-formed minerals in the clast. Extreme variations in fayalite HREE abundances and HREE depletion in sodic plagioclase and phosphate for MET 01210 can be explained by co-crystallization of a late-stage mineral that strongly fractionates the REE. Zircon is especially effective for fraction-

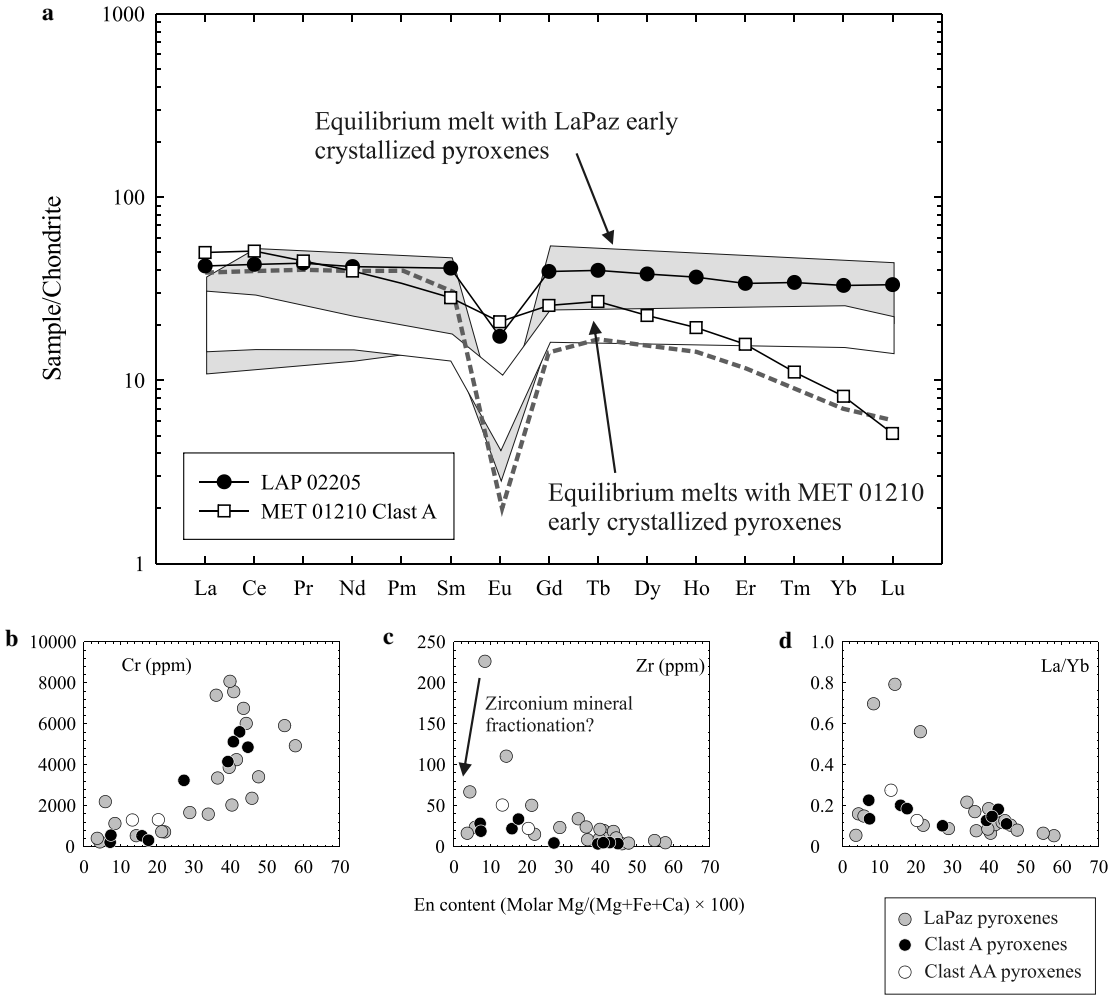

Fig. 16. (a) CI chondrite-normalized REE abundances for LAP 02205 whole-rock measured by ICP-MS (Day et al., 2006), equilibrium liquid compositions for zircons in sample 14001, 7003 (thick stippled line—from Snyder et al., 1993), and modal recombination of whole-rock REE abundances in MET 01210 clast A and AA. Superimposed are fields of melts in equilibrium with earliest formed pyroxenes in both basalts using partition co-efficient data from McKay et al. (1986). LaPaz pyroxene equilibrium melts agree well with the overall whole-rock composition of LAP 02205 (Anand et al., 2006), whereas clast A pyroxene equilibrium melts do not agree with clast whole-rock REE recombinations. This difference may be attributed to late-stage crystallization of zircon or zirconium-rich minerals capable of fractionating the REE. Enstatite content versus Cr (b), Zr (c) and La/Yb (d) for pyroxenes in LAP 02205 and MET 01210. Data are from this study and Anand et al. (2006).

ating the REE, with partition coefficients for HREE up to 1000 times greater than that of the LREE (e.g., Snyder et al., 1993). Lunar zircons are commonly found as loose grains in soils, breccias and "sawdust," but have rarely been documented in mare basalt rock specimens (Meyer et al., 1991). However, zirconium-rich minerals have been recognized within the mesostases of some mare basalt meteorites (e.g., Day et al., 2006; Zeigler et al., 2005b). Snyder et al. (1993) considered that mare basalts were unlikely to become saturated in zirconium because it can be compatible in opaque oxides (ilmenite, ulvöspinel). However, the calculated equilibrium liquid compositions for zircon in Apollo 14001, 7003 are very similar to the calculated modal whole-rock composition of clast A and strongly support the notion of late-stage zircon crystallization in the evolved parental liquids of the MET 01210 basalt clasts. The lack of zircon, or zirconium-rich minerals observed in the basalt clasts is likely a function of the lack of preserved grains, demonstrating the grain size to surface area effect.

Despite having different textures, Clasts A and AA are clearly from a similar, if not identical sources and may even come from the same lunar basaltic lava flow. The similar incompatible element abundances and patterns for pyroxenes and plagioclases in these clasts support the notion that they are from the same source. Textural differences between basalt clasts do not impede 'pairing,' because variations in texture may simply reflect different cooling histories for products of the same magmatic system. The basalt clasts in MET 01210 appear to come from similar source regions as evolved mare basalts that have 'Fenner-trend' enrichments such as NWA 773, A-881757 or Y-793169. For example, Fe-rich clasts (e.g., BB, H), symplectic growths and large fayalites in MET 01210 are strongly reminiscent of fayalitic bearing gabbros and fayalitic granite rocks in the breccia of NWA 773 (Fagan et al., 2003). The similarities of samples such as MET 01210, A-881757, Y-793169, NWA 773, NWA 032 and the LaPaz mare basalts may indicate similar sources for these meteorites. NWA 032, NWA 773 and the LaPaz mare basalts are all relatively young, and incompatible-element-enriched (2.8–3.0 Ga; Fagan et al., 2002; Borg et al., 2004; Anand et al., 2006) whereas A-881757 and Y-793169 are more ancient and ferroan (3.7 Ga; e.g., Fernandez et al., 2005 and references therein). Whole-rock trace element and geochronology studies of MET 01210 will allow further appraisal regarding possible relations this meteorite has with younger incompatible-element-rich and older ferroan mare basalts.

4.3. A rare clast in PCA 02007—primary evidence for chondritic lunar impactors?

Clast T8 is an unusual clast, unlike any previously documented in a lunar meteorite. Olivine cores in T8 are significantly more forsteritic, CaO-rich and have different Fe/Mn ratios compared with typical olivine-rich lunar cumulates (NWA 773, cataclastic dunites, e.g., 72415 and 72418; Fagan et al., 2003; Dymek et al., 1975) or olivines found in lunar breccias or basalts, and share similarities with chondritic olivines (Figs. 13, 15a). In addition, pentlandite and pyrrhotite assemblages, although common in stony iron meteorites (e.g., Rubin, 1997) do not occur in lunar rocks, and the metal compositions documented in T8 (Fig. 7) are also typical of chondritic meteorites. Finally, the minerals and reconstructed whole-rock have low refractory element abundances, nearly flat chondritic-relative REE patterns, and, with the exception of plagioclase, lack large positive- or negative-Eu anomalies (Fig. 13), features not considered typical of lunar rocks.

Chondrule-like objects have been discovered, often in fairly high abundances (5–10% in 14315 and 14318), in Apollo 11, 14 and 16 and Luna 16 regolith breccias and in some feldspathic regolith breccia meteorites (e.g., Fredricksson et al., 1970; Keil et al., 1972; King et al., 1972; Kurat et al., 1972; Koeberl et al., 1991; Symes et al., 1998). However, these objects are texturally different from clast T8 and have aluminous compositions with low MgO that indicate an origin from anorthositic, noritic and troctolitic precursor rocks (Kurat et al., 1972; Symes et al., 1998) and are not high in MgO and low in Al_2O_3 like clast T8. In this respect, these objects are more similar to the impact glasses documented in PCA 02007 (Fig. 8f and h). These chondrule-like objects are thought to originate through high velocity impact melting and moderately slow cooling; their bulk constituents are not meteoritic in origin.

Fragments of meteorites have been recognized in lunar soils and, with the exception of a carbonaceous chondrite in Bench Crater (12037,188—McSween, 1976; Zolensky, 1997) and a tentatively described enstatite chondrite discovered in Apollo soil sample 15602 (Haggerty, 1972), are almost exclusively kamacite-taenite metal, sometimes containing troilite and/or schreibersite (Papike et al., 1998). The three so far described exogenous chondrite fragments differ greatly from one another, with Clast T8 containing abundant olivine, whereas the Bench Crater meteorite and 15602 contain no preserved olivine. In detail, the Bench Crater meteorite contains 59 vol % matrix material, 20 vol % pyroxene, 12 vol % magnetite and 9 vol % troilite (McSween, 1976), whereas the clast in 15602 contains ~75 vol % enstatite, ~20 vol % kamacite, ~2 vol % silica and ~3 vol % troilite, schreibesite and niningerite (Haggerty, 1972). Taylor et al. (2004b) suggested that clast T8 could be a hitherto unknown type of chondrule. If so, it partially resembles porphyritic olivine plagioclase-rich chondrules similar to those described by Krot and Keil (2002a) and Krot et al. (2002b). The major difference between the clast and typical chondrules is the angular and fragmented nature of the silicate minerals and the absence of pyroxene. These features may be ascribed to intense shock and partial reworking of the clast.

One difficulty with a chondrule origin for T8 is the extreme olivine zonation in the clast. Some of the variation

may be due to reworking and interaction with lunar regolith constituents after impact. Almost all of the clasts in PCA 02007 have metamorphic textures, and the texture of clast T8 also appears 'pseudo-brecciated.' In this regard, it is important to note that the shape of the clast indicates some degree of deformation, possessing conchoidal outer surfaces (Fig. 8a). Partial melting and mixing between meteoritic and lunar material, or diffusion of certain elements at high temperatures may lead to partial equilibration and resorbtion subsequent to impact. However, extreme Fe zonation and high Fe/Mn ratios of olivine rims, and the positive Eu anomalies in T8 plagioclase are not entirely due to partial equilibration with regolith constituents in PCA 02007. The most susceptible material for high temperature element diffusion would be glass. However, glass in clast T8 is incompatible-element enriched with a broadly flat REE pattern, typical of ordinary chondrule glasses (e.g., Alexander, 1994), arguing against equilibration with lunar regolith (Fig. 13). This observation is further supported by the low refractory element contents in clast T8, which are similar to those of 12037,188 (McSween, 1976). Finally, elevated Fe/Mn ratios in the rims of olivines do not require extensive equilibration or partial mixing with lunar materials, and can be mostly accounted for by closed-system fractional crystallization. For example, there is a positive correlation with Fe and Fe/Mn ratio for chondrule olivines, with the most FeO-rich olivines possessing the highest Fe/Mn ratios (Fe/Mn up to 147; Data from Table A.3.1 of Brearley and Jones, 1998), compared with Mg-rich chondrule olivines that have low Fe/Mn ratios (typically < 20). It is notable that low forsterite olivines plot along the lunar Fe/Mn trend as shown by PCA 02007 and MET 01210 olivine populations. In contrast, the majority of forsteritic olivines in T8 plot along a Fe/Mn fractionation trend more typical of that exhibited in chondrules (Fig. 15b). This observation indicates possible interaction and element diffusion for the outer few microns of clast T8 olivines with lunar material. The lack of lunar Fe/Mn ratios in the innermost portions of the olivines ($Fo_{80–100}$) in clast T8 suggests the bulk of the olivine compositions are not lunar in origin, and are more typical of chondrule Fe/Mn fractionation trends.

To explain the zonation in olivine from $Fo_{80–100}$ (i.e., those that have not undergone chemical interaction with the lunar regolith), it may be possible that clast T8 represents a partially metamorphosed chondrule and that the bimodal distribution of olivines reflects a mixture of initial chondritic Type I (FeO-poor, $Fa < 10$) and Type II (FeO-rich $Fa > 10$) compositions (Hewins, 1997), with the Eu anomalies in the plagioclase explained by changing oxygen fugacities in the melt droplet (Jones, 1990). For this to occur, a process such as metasomatism would have had to modify the almost pure forsterite to Fe-rich rims (e.g., Taylor et al., 2004b). An alternative possibility is that the observed olivine zonation has occurred through extreme closed-system fractional crystallization (Jones, 1990). The Fe zonation in the olivine does share some similarities with ordinary chondrules such as those found in LL3.0-ordinary chondrite, Semarkona. The olivine grains in some Semarkona chondrules are of similar morphology and size to grains in clast T8, and they exhibit zonation to Fe-rich rims (Jones, 1990).

The normal zonation in clast T8 olivine grains can be used to generate cooling rate information assuming a peak temperature. At a peak temperature of 1673 K (Hewins, 1997), the diffusion rate is similar to typical ferromagnesian chondrules ($\sim$1000 °C/h; Alexander, 1994). Krot et al. (2002b) assumed a lower ambient temperature due to the presence of calcium–aluminium rich inclusions (CAIs) in the plagioclase-rich chondrules that they studied. Despite CAIs being absent from clast T8, if we employ a lower ambient temperature (1473 K) the diffusion rate is $\sim$42 °C/h. It is unclear if such high cooling rates are feasible after impact and incorporation into the lunar regolith, and these calculated temperatures are similar to those of Fe/Mg diffusion profiles of chondrule olivines.

On the basis of arguments made here, we suggest that clast T8 is an exogenous (i.e., meteoritic) component in PCA 02007 that has been preserved, either through low velocity or oblique impact of its parental impactor, within the lunar regolith. Clast T8 has similarities to both ordinary and carbonaceous chondrules, especially plagioclase-rich chondrules in CV chondrites. Although we cannot discount the possibility of some reworking and resorbtion of meteoritic and lunar material, many of the features of clast T8 can be explained by processes external to the Moon. For example, Fe-enrichment of olivine may be explained by interaction with lunar materials ($Fo_{<80}$) and extreme closed-system fractional crystallization ($Fo_{>80}$), similar to that observed in H- and LL-type ordinary chondrites. We suggest that this is the second well documented silicate impactor preserved on the Moon after the Bench Crater meteorite 12037,188 (McSween, 1976) and, as such, has important implications for future meteorite finds on planetary bodies and for the identification of lunar impactor populations. Large craters and the presence of meteoritic metal fragments in lunar soil and regolith clearly attest to a violent history of projectiles striking the Moon. However, the main evidence for lunar impactors of chondritic composition has been from highly siderophile element studies of impact melt breccias (e.g., Norman et al., 2002). Rocky impactors were thought to largely volatilize upon striking the Moon. This is unlike the Earth where atmospheric friction reduces small impactor velocities. The presence of clasts such as PCA 02007, T8 and 12037,188 indicates that meteorite delivery systems to the Moon may be favorable to further finds of meteorites, allowing comparison with the well characterized meteorite flux of the present-day Earth. Based on the clasts PCA 02007,T8, 12037,188 and the putative enstatite chondrite in soil 15602 (Haggerty, 1972), it seems that the full range of

main chondritic groups (enstatite, ordinary, carbonaceous) have been recognized in the lunar regolith. However, based on the mineralogy of these fragments, and the highly siderophile element ratios of impact melt breccias, it is possible that differences may exist between the ancient meteorite flux to the Moon and that of the present-day Earth.

4.3.1. Comparisons with other lunar rocks

As noted by numerous studies, MET 01210 has a whole-rock composition unlike any previously described predominantly basaltic breccia (Fig. 14a–c; Arai et al., 2005; Patchen et al., 2005; Zeigler et al., 2005a), although it has been considered similar to NWA 3136 (Korotev and Irving, 2005). Mineralogically MET 01210 has been noted to be very similar to both the 3.7 Ga VLT mare basalt meteorites, A-881757 and Y-793169 (Arai et al., 2005), the 2.8–3.0 Ga LaPaz basalts, NWA 032 and NWA 773 (Section 4.3) and to Luna 24 VLT basalts (Arai et al., 2005; Patchen et al., 2005). This is unsurprising considering the overall low titanium to very low titanium nature of predominantly basaltic lunar meteorites discovered to date. The higher whole-rock Ti content and different mineralogical fractionation trends of MET 01210 versus other predominantly basaltic brecciated meteorites (EET 87521/96008; Y-793274; QUE 94281) contrasts with the similar pyroxene exsolution lamellae found in these clasts and suggests common shallow, slowly cooled components in these meteorites. On the basis of petrological and geochemical observations, MET 01210 provides information on a source region of the Moon similar to the evolved low-Ti mare basalts. Cogent arguments for the relations of this meteorite to other predominantly basaltic meteorites will be more accurately made with exposure ages for the meteorite and crystallization ages for some of the basalt clasts.

PCA 02007 has a number of similarities to previously described feldspathic regolith breccia meteorites and has been suggested to be compositionally paired with Y-791197 (Zeigler et al., 2004). It is also very similar to Mg-rich feldspathic regolith breccias such as ALHA 81005. The high Mg content of PCA 02007 may, in part, be due to the relatively high percentage volume of low Ti basaltic clasts in the meteorite, but is likely to be dominated by the significant quantity of 'high magnesian suite-like' noritic and troctolitic lithologies. In this respect, PCA 02007 is similar to lunar granulites thought to be from precursor noritic anorthosites (Lindstrom and Lindstrom, 1986). Regolith breccia meteorites such as PCA 02007 are particularly useful because they are likely to represent average compositions of their source regions and so provide a better understanding of the lunar highlands. Mg-rich noritic anorthosite rocks have been proposed as major constituents of the lunar crust (Jolliff et al., 2000) and studies of feldspathic regolith breccias have also supported this view (Korotev et al., 2003).

The geochemical similarities of PCA 02007 to other feldspathic regolith breccia meteorites also supports a high-Mg/Fe Feldspathic Highlands Terrane (Jolliff et al., 2000) for the Moon and lies within the estimated 'lunar crust' composition of Korotev et al. (2003). These authors have provided persuasive arguments that the magnesian granulite breccias (including feldspathic regolith breccia meteorites) do not solely originate from the Procellarum KREEP Terrane (Jolliff et al., 2000) and must be distributed widely. Although this makes identifying possible source regions for PCA 02007 difficult, it must be similar to some of the other high-Mg/Fe feldspathic regolith breccia meteorites. Mixing of components has also led to a lack of possible meteorite pairing criterion for feldspathic regolith breccias (Korotev, 2005), although they all appear to come from source regions of the Moon that are noritic and feldspathic with low incompatible element abundances.

Studies of lunar feldspathic regolith breccia meteorites provide geochemical confirmation that ferroan anorthosites occur in all feldspathic lunar breccias, as well as in predominantly mare basalt breccias (e.g., Clast M, MET 01210, clasts in QUE 92481, EET 96008; Jolliff et al., 1998; Anand et al., 2003); however, it is also the coexistence of noritic and troctolitic lithologies with anorthosite that accounts for the high Mg/Fe ratios of some of the magnesian granulite breccias (Lindstrom and Lindstrom, 1986) and feldspathic regolith breccia meteorites. An important uncertainty arising in interpreting feldspathic regolith breccias, is that it remains unclear how much material is from local material versus from further locales. Delano (1991) studied glasses in feldspathic lunar meteorites ALHA 81005, MAC 88105 and a Apollo 16 regolith, 64001 and suggested that high-Ti glasses were transported from distances in excess of 300 km to the Apollo 16 site. Delano (1991) also demonstrated that, like glass spherules in PCA 02007, the most common heritage for the glasses in these rocks was found to be as quenched droplets of impact melt that should represent the bulk composition of the original target material (Delano, 1991).

Assuming that the diversity in glass compositions reflects target material compositions, it is apparent that PCA 02007, along with other feldspathic regolith breccia meteorites, sample a wide range of lithologies such that they overlap the entire range of whole-rock feldspathic breccia meteorite compositions (Fig. 5). This diversity in target material for glasses in PCA 02007 confirms that feldspathic highland regolith breccias are probably the most representative rocks of the lunar crust making them suitable for comparison with remote sensing data and as analogs for the Feldspathic Highlands Terrane. On the basis of clast variety in PCA 02007 and other feldspathic lunar meteorites it is unclear whether the bulk Mg/Fe-rich compositions of these meteorites are a direct reflection of the gross crustal composition (i.e., a stratified crust or a ferroan-rich crust intruded by high-magnesian suite material), or are simply an amalgamation of high-magnesian suite, ferroan anorthosite and mare basalt components mixed by impact-related processes on the lunar surface.

5. Summary

Lunar meteorites MET 01210 and PCA 02007 are breccias from the mare and the Feldspathic Highlands Terrane, respectively. MET 01210 is composed predominantly of fractionated low-Ti basaltic material that may have undergone late-stage fractional crystallization of zircon or a zirconium-rich mineral, similar to the process suggested by Snyder et al. (1993). Some of the features of MET 01210 are similar to other predominantly basaltic lunar breccias and include coarse pyroxene exsolution, symplectic breakdown textures and fractional crystallization, consistent with the clasts in this meteorite forming in a ponded lava lake or in a thick low-Ti basalt flow. The presence of anorthositic metamorphic clasts and agglutinate indicate a small regolith component but otherwise MET 01210 can be considered to be an immature predominantly basaltic glassy matrix regolith breccia meteorite from a mare region.

PCA 02007 is composed predominantly of metamorphic feldspathic clasts, agglutinate, impact-glasses and noritic, troctolitic and noritic anorthosite clasts, however, there are a significant number of basaltic clasts with both mare and non-mare (low-Ca pyroxene) affinities. PCA 02007 shares many features with other feldspathic regolith breccias, including a high Mg/Fe whole-rock composition, glass spherules, agglutinate fragments and a diverse clast inventory spanning the compositional ranges of ferroan anorthosite and high-magnesian suite rocks. Some of the mare basalt fragments in this sample are extremely fractionated and, in this respect, are similar to mare basalt clasts in MET 01210. Another similarity with these meteorites is the presence of coarse pyroxene exsolution features. PCA 02007 supports previous studies of feldspathic lunar meteorites that suggest an aluminous crust for the Moon with compositions more similar to magnesian granulite breccias than ferroan anorthosites (Korotev et al., 2003). What remains unclear, however, is whether these Mg/Fe-rich compositions are a direct reflection of the gross crustal composition or are simply an amalgamation of high-magnesian suite, ferroan anorthosite and mare basalt components. Unraveling what the individual components in feldspathic lunar meteorites represent remains an important petrological challenge.

A significant clast in PCA 02007 is a 'chondrule-like' fragment unlike any previously described material found in a lunar rock. This clast is porphyritic with equant olivines that have forsterite-rich cores ($Fo_{>98}$), extreme normal zonation to more fayalitic rims ($Fo_{>44}$) and a mineral assemblage with rare earth element abundances unlike previously described lunar material and more like chondrules found in ordinary or carbonaceous chondrites. Its discovery and description are important for understanding the composition of lunar impactors. The presence of this clast indicates that meteorite delivery systems to the Moon may be favorable to further finds of meteorites on airless bodies, allowing comparison with the well characterized meteorite flux of the Earth, helping to elucidate the late accretionary history of the inner solar system.

Acknowledgments

We dedicate this paper to the memory of Larry Haskin. We thank MWG for the provision of samples for petrological studies and C. Alexander for useful suggestions that helped to focus our arguments on the origin of clast T8. Reviews by R. Zeigler, C. Koeberl and an anonymous improved the quality of this work. This research has been supported through NASA Cosmochemistry Grants NNG05GG03G and NNG04GG49G.

Associate editor: Christian Koeberl

References

Alexander, C.M.O'D., 1994. Trace element distributions within ordinary chondrite chondrules: implications for chondrule formation conditions and precursors. *Geochim. Cosmochim. Acta* **58**, 3451–3467.

Alibert, C., Norman, M.D., McCulloch, M.T., 1994. An ancient Sm-Nd age for a ferroan noritic anorthosite clast from lunar breccia 67016. *Geochim. Cosmochim. Acta* **58**, 2921–2926.

Anand, M., Taylor, L.A., Neal, C.R., Snyder, G.A., Patchen, A., Sano, Y., Terada, K., 2003. Petrogenesis of lunar meteorite EET 96008. *Geochim. Cosmochim. Acta* **67**, 3499–3518.

Anand, M., Taylor, L.A., Floss, C., Neal, C.R., Terada, K., Tanigawa, S., 2006. Petrology and geochemistry of LAP 02205: a new low-Ti mare basalt meteorite. *Geochim. Cosmochim. Acta* **70**, 246–264.

Anders, E., Grevesse, N., 1989. Abundances of the elements: meteoritic and solar. *Geochim. Cosmochim. Acta* **53**, 197–214.

Arai, T., Takeda, H., Warren, P.H., 1996. Four lunar mare meteorites: crystallization trends of pyroxenes and spinels. *Meteor. Planet. Sci.* **31**, 877–892.

Arai, T., Warren, P.H., 1999. Lunar meteorite Queen Alexandra Range 94281: Glass compositions and other evidence for launch pairing with Yamato 793274. *Meteor. Planet. Sci.* **34**, 209–234.

Arai, T., Misawa, K., Kojima, H., 2005. A new lunar meteorite MET 01210: mare breccia with a low-Ti ferrobasalt. *Lunar Planet. Sci.* **XXXVI**, CD-ROM #2361 [Abs.].

Bence, A.E., Papike, J.J., 1972. Pyroxenes as recorders of lunar basalt petrogenesis: chemical trends due to crystal-liquid interaction. *Proc. Lunar Sci. Conf.* **3rd**, 431–469.

Borg, L.E., Shearer, C.K., Asmerom, Y., Papike, J.J., 2004. Prolonged KREEP magmatism on the Moon indicated by the youngest dated lunar igneous rock. *Nature* **432**, 209–211.

Brearley, A.J., Jones, R.H., 1998. Chondritic meteorites. In: Papike, J.J. (Ed.), *Planetary Materials. Reviews in Mineralogy*, vol. 36. Mineralogical Society of America, Washington, pp. 3.1–3.39.

Brett, R., Butler Jr., P., Meyer Jr., C., Reid, A.M., Takeda, H., Williams, R., 1971. Apollo 12 igneous rocks 12004, 12008, 12009, and 12022: a mineralogical and petrological study. *Proc. Lunar Sci. Conf. 2nd*, 301–317.

Brown, G.M., Emeleus, C.H., Holland, J.G., Peckett, A., Phillips, R., 1971. Picrite basalts, ferrobasalts, feldspathic norites, and rhyolites in a strongly fractionated lunar crust. *Proc. Lunar Sci. Conf. 2nd*, 583–600.

Brown, G.M., Emeleus, C.H., Holland, J.G., Peckett, A., Phillips, R., 1972. Mineral-chemical variations in Apollo 14 and Apollo 15 basalts and granitic fractions. *Proc. Lunar Sci. Conf. 3rd*, 141–157.

Carlson, R.W., Lugmair, G.W., 1988. The age of ferroan anorthosite 60025: oldest crust on a young Moon? *Earth Planet. Sci. Lett.* **90**, 119–130.

Coish, R.A., Taylor, L.A., 1978. Mineralogy and petrology of basaltic fragments from the Luna 24 drill core. In: Merrill, R.B., Papike, J.J. (Eds.), *Mare Crisium: The view from Luna 24*. Pergamon Press, New York, pp. 403–417.

Day, J.M.D., Taylor, L.A., Floss, C., Patchen, A.D., Schnare, D.W., Pearson, D.G., 2006. Comparative petrology, geochemistry and petrogenesis of evolved, low-Ti lunar mare basalt meteorites from the LaPaz icefield, Antarctica. *Geochim. Cosmochim. Acta* **70**, 1581–1600.

Delaney, J.S., 1989. Lunar basalt breccia identified among Antarctic meteorites. *Nature* **342**, 889–890.

Delano, J.W., 1986. Pristine lunar glasses: criteria, data, and implications. *Proc. Lunar Planet. Sci. Conf., 16th, J. Geophys. Res. Supplement* **90**, D201–D213.

Delano, J.W., 1991. Geochemical comparison of impact glasses from lunar meteorites ALHA81005, MAC 88105 and Apollo 16 regolith 64001. *Geochim. Cosmochim. Acta* **55**, 3019–3029.

Dickinson, T., Taylor, G.J., Keil, K., Schmitt, R.A., Hughes, S.S., Smith, M.R., 1985. Apollo 14 aluminous mare basalts and their possible relationship to KREEP. *Proc. Lunar Planet. Sci. Conf., 15th, J. Geophys. Res. Supplement* **90**, C37–C365.

Drake, M.J., Newsom, H.E., Capobianco, C.J., 1989. V, Cr and Mn in the earth, moon, EPB, and SPB and the origin of the moon: experimental studies. *Geochim. Cosmochim. Acta* **53**, 2101–2111.

Dymek, R.F., Albee, A.L., Chodos, A.A., 1975. Comparative petrology of lunar cumulate rocks of possible primary origin: Dunite 72415, troctolite 76535, norite 78235 and anorthosite 62237. *Proc. Lunar. Sci. 6th*, 301–341.

Dymek, R.F., Albee, A.L., Chodos, A.A., Wasserburg, G.J., 1976. Petrography and isotopically-dated clasts in the Kapoeta howardite and petrologic constraints on the evolution of its parent body. *Geochim. Cosmochim. Acta* **40**, 1115–1130.

Fagan, T.J., Taylor, G.J., Keil, K., Bunch, T.E., Wittke, J.H., Korotev, R.L., Jolliff, B.L., Gillis, J.J., Haskin, L.A., Jarosewich, E., Clayton, R.N., Mayeda, T.K., Fernandez, V.A., Burgess, R., Turner, G., Eugster, O., Lorenzetti, S., 2002. Northwest Africa 032: product of lunar volcanism. *Meteor. Planet. Sci.* **37**, 371–394.

Fagan, T.J., Taylor, G.J., Keil, K., Hicks, T.L., Killgore, M., Bunch, T.E., Wittke, J.H., Mittlefehldt, D.W., Clayton, R.N., Mayeda, T.K., Eugster, O., Lorenzetti, S., Norman, M.D., 2003. Northwest Africa 773: lunar origin and iron-enrichment trend. *Meteor. Planet. Sci.* **38**, 529–554.

Fernandez, V.A., Morris, A., Burgess, R., 2005. New Ar–Ar age determinations for the lunar mare basalts Asuka 881757 and Yamato 793169. *Lunar Planet. Sci. Conf.* **XXXVI**, CD-ROM 1002 [Abs.].

Floss, C., James, O.B., McGee, J.J., Crozaz, G., 1998. Lunar ferroan anorthosite petrogenesis: clues from trace element distributions in FAN subgroups. *Geochim. Cosmochim. Acta* **62**, 1255–1283.

Fredricksson, K., Nelen, J., Melson, W.G., Henderson, E.P., Anderson, C.A., 1970. Lunar glasses and micro-breccias: properties and origin. *Science* **167**, 664–666.

Goldstein, J.I., Yakowitz, H., 1971. Metallic inclusions and metal particles in the Apollo 12 lunar soil. *Proc. Lunar. Sci. Conf. 2nd*, 177–191.

Gnos, E., Hofmann, B.A., Al-Kathiri, A., Lorenzetti, S., Eugster, O., Whitehouse, M.J., Villa, I.M., Jull, A.J.T., Elkenberg, J., Spettel, B., Krähenbühl, U., Franchi, I.A., Greenwood, R.C., 2004. Pinpointing the source of a lunar meteorite: implications for the evolution of the Moon. *Science* **305**, 657–659.

Grove, T.L., Bence, A.E., 1977. Experimental study of pyroxene-liquid interaction in quartz-normative basalt 15597. *Proc. Lunar Sci. Conf.* **8**, 1549–1579.

Haggerty, S.E., 1972. An enstatite chondrite from Hadley Rille. In: Chamberlain, J.W., Watkins, C. (Eds.) The Apollo 15 lunar samples. Lunar Science Institute, Houston, Texas, pp. 85–87 [Abs.].

Hewins, R.H., 1997. Chondrules. *Annu. Rev. Earth Planet. Sci.* **25**, 61–83.

Hill, D.H., Boynton, W.V., Haag, R.A., 1991. A lunar meteorite found outside the Antarctic. *Nature* **352**, 614–617.

Hsu, W., 1995. Ion microprobe studies of the petrogenesis of enstatite chondrites and eucrites. Ph.D. Thesis. Washington University.

Huber, H., Warren, P.H., 2005. MET 01210: Another lunar mare meteorite (regolith breccia) with extensive pyroxene exsolution and not part of the YQ launch pair. *Lunar Planet. Sci.* **XXXVI**, CD-ROM #2401 [Abs.].

Hunter, R.H., Taylor, L.A., 1983. The magma ocean from the Fra Mauro shoreline: an overview of the Apollo 14 crust. *Proc. Lunar Planet. Sci. Conf. 13th*, A591–A602.

Jolliff, B.L., Korotev, R.L., Haskin, L.A., 1991. A ferroan region of the lunar highlands as recorded in meteorites MAC 88104 and MAC 88105. *Geochim. Cosmochim. Acta* **55**, 1051–1071.

Jolliff, B.L., Haskin, L.A., Korotev, R.L., Colson, R.O., Wadwha, M., 1993. Partitioning in REE-saturated minerals: theory, experiment, and modeling of whitlockite, apatite, and evolution of lunar residual magmas. *Geochim. Cosmochim. Acta* **57**, 4069–4094.

Jolliff, B.L., Korotev, R.L., Rockow, K.M., 1998. Geochemistry and petrology of lunar meteorite Queen Alexander Range 94281, a mixed mare and highland regolith breccia, with special emphasis on very-low-titanium components. *Meteor. Planet. Sci.* **33**, 581–601.

Jolliff, B.L., Gillis, J.J., Haskin, L.A., Korotev, R.L., Wieczorek, M.A., 2000. Major lunar crustal terranes: surface expressions and crust–mantle origins. *J. Geophys. Res.* **105**, 4197–4216.

Jones, R.H., 1990. Petrology and mineralogy of Type II, FeO-rich chondrules in Semarkona (LL3.0): origin by closed-system fractional crystallization, with evidence for supercooling. *Geochim. Cosmochim. Acta* **54**, 1785–1802.

Keil, K., Kurat, G., Prinz, M., Green, J.A., 1972. Lithic fragments, glasses and chondrules from Luna 16 fines. *Earth Planet. Sci. Lett.* **13**, 243–256.

King, E.A., Carman, M.F., Butler, J.C., 1972. Chondrules in Apollo 14 samples: implications for the origin of chondritic meteorites. *Science* **175**, 59–60.

Koeberl, C., Kurat, G., Brandstätter, F., 1991. MAC 88105—a regolith breccia from the lunar highlands: mineralogical, petrological and geochemical studies. *Geochim. Cosmochim. Acta* **55**, 3073–3087.

Koeberl, C., Kurat, G., Brandstätter, F., 1996. Mineralogy and geochemistry of lunar meteorite Queen Alexandra Range 93069. *Meteor. Planet. Sci.* **31**, 897–908.

Korotev, R.L., 2005. Lunar geochemistry as told by lunar meteorites. *Chemie der Erde* **65**, 297–346.

Korotev, R.L., Irving, A.J., 2005. Compositions of three lunar meteorites: Meteorite Hills 01210, Northeast Africa 001 and Northwest Africa 3136. *Lunar Planet. Sci.* **XXXVI**, CD-ROM #1220 [Abs.].

Korotev, R.L., Jolliff, B.L., Zeigler, R.A., Gillis, J.J., Haskin, L.A., 2003. Feldspathic lunar meteorites and their implications for compositional remote sensing of the lunar surface and the composition of the lunar crust. *Geochim. Cosmochim. Acta* **67**, 4895–4923.

Krot, A.N., Keil, K., 2002a. Anorthite-rich chondrules in CR and CH carbonaceous chondrites: genetic link between calcium–aluminium-rich inclusions and ferromagnesian chondrules. *Meteor. Planet. Sci.* **37**, 91–111.

Krot, A.N., Hutcheon, I.D., Keil, K., 2002b. Plagioclase-rich chondrules in the reduced CV chondrites: evidence for complex formation history and genetic links between calcium–aluminium-rich inclusions and ferromagnesian chondrules. *Meteor. Planet. Sci.* **37**, 155–182.

Kurat, G., Keil, K., Prinz, M., Nehru, C.E., 1972. Chondrules of lunar origin. *Proc. Lunar Sci. 3rd*, 707–721.

Lindsley, D.H., Andersen, D.J., 1983. A two-pyroxene thermometer. *Proc. Lunar Planet. Sci. Conf., 13th, J. Geophys. Res. Supplement* **88**, A887–A906.

Lindsley, D.H., Papike, J.J., Bence, A.E., 1972. Pyroxferroite: breakdown at low pressure and high temperature. *Lunar Sci. Conf.* 3rd, 483–485 [Abs.].

Lindstrom, M.M., Lindstrom, D.J., 1986. Lunar granulites and their precursor anorthositic norites of the early lunar crust. *Proc. Lunar Planet. Sci. Conf., 16th, J. Geophys. Res. Supplement* **90**, D262–D276.

Lofgren, G.E., Donaldson, C.H., Williams, R.J., Mullins, O.J., Usselman, T.M., 1974. Experimentally reproduced textures and mineral chemistry

of Apollo 15 quartz normative basalts. *Proc. Lunar Sci. Conf. 5th*, 549–567.

Lu, F., Taylor, L.A., Jin, Y., 1989. Basalts and Gabbros from Mare Crisium: Evidence for extreme fractional crystallization. *Proc. Lunar Planet. Sci. Conf. 19th*, 199–207.

McCoy, T., Welzenbach, L., 2003. PCA 02007. In: Satterwhite, C., Righter, K. (Eds.), Antarctic Meteorite Newsletter, vol. 26, No. 2.

McCoy, T., Welzenbach, L., 2004. MET 01210. In: Satterwhite, C., Righter, K. (Eds.), Antarctic Meteorite Newsletter, vol. 27, No. 1.

McKay, G., Wagstaff, K., Yang, S.-R., 1986. Clinopyroxene REE distribution coefficients for shergottites: the REE content of the Shergotty melt. *Geochim. Cosmochim. Acta* **50**, 927–937.

McSween Jr., H.Y., 1976. A new type of chondrite meteorite found in lunar soil. *Earth Planet. Sci. Lett.* **31**, 193–199.

Meyer, C., Galindo, C., Yang, V., 1991. Lunar zircon. *Lunar Planet. Sci.* **XXII**, 895–896 [Abs.].

Neal, C.R., 2001. Interior of the Moon: the presence of garnet in the primitive deep lunar mantle. *J. Geophys. Res. Planet.* **106**, 27865–27885.

Neal, C.R., Taylor, L.A., 1991. Evidence for metasomatism of the lunar highlands and the origin of whitlockite. *Geochim. Cosmochim. Acta* **55**, 2965–2980.

Norman, M.D., Taylor, S.R., 1992. Geochemistry of lunar crustal rocks from breccia 67016 and the composition of the Moon. *Geochim. Cosmochim. Acta* **56**, 1013–1024.

Norman, M.D., Taylor, G.J., Keil, K., 1991. Additional complexity in the lunar crust: petrology of sodic anorthosites and sulfur-rich, ferroan noritic anorthosites. *Geophys. Res. Lett.* **18**, 2081–2084.

Norman, M.D., Bennett, V.C., Ryder, G., 2002. Targeting the impactors: highly siderophile element signatures of lunar impact melts from Serenitatis. *Earth Planet. Sci. Lett.* **202**, 217–228.

Papike, J.J., 1998. Comparative planetary mineralogy: chemistry of melt-derived pyroxene, feldspar and olivineIn. In: Papike, J.J. (Ed.), *Planetary Materials*, vol. 36. Reviews in Mineralogy, Mineralogical Society of America, Washington, p. 7.1.

Papike, J.J., Ryder, G., Shearer, C.K., 1998. Lunar samples. In: Papike, J.J. (Ed.), *Planetary Materials*, vol. 36. Reviews in Mineralogy, Mineralogical Society of America, Washington, pp. 5.1–5.23.

Patchen, A.D., Taylor, L.A., Day, J.M.D. 2005. Mineralogy and petrography of lunar mare regolith breccia meteorite MET 01210. *Lunar Planet. Sci.* **XXXVI**, CD-ROM #1411 [Abs.].

Rubin, A.E., 1997. Mineralogy of meteorite groups. *Meteor. Planet. Sci.* **32**, 231–247.

Shafer, J., Neal, C.R., Castillo, P., 2004. Compositional variability in lavas from the Ontong Java Plateau: results from clasts within the volcaniclastic sequence of Ocean Drilling Program Leg 192, Site 1184. In: Fitton, J.G., Mahoney, J.J., Wallace, P.J., Saunders, A.D. (Eds.), Origin and evolution of the Ontong Java Plateau. Geol. Soc. London, Spec. Pub. 229, pp. 333–351.

Snyder, G.A., Taylor, L.A., Crozaz, G., 1993. Rare earth element selenochemistry of immiscible liquids and zircon at Apollo 14: an ion probe study of evolved rocks on the Moon. *Geochim. Cosmochim. Acta* **57**, 1143–1149.

Snyder, G.A., Taylor, L.A., Patchen, A., 1999. Lunar meteorite EET 96008, Part 1, Petrology and mineral chemistry: evidence of large-scale, late-stage fractionation. *Lunar Planet. Sci.* **XXX** CD-ROM #1499 [Abs.].

Stöffler, D., Marvin, U.B., Simonds, C.H., Warren, P.H., 1980. Recommended classification and nomenclature of lunar highland rocks—a committee report. In: Papike, J.J., Merrill, R.B. (Eds.), *Proc. Conf. Lunar Highlands Crust*. Pergamon Press, pp. 51–70.

Symes, S.J.K., Sears, D.W.G., Akridge, D.G., Huang, S., Benoit, P.H., 1998. The crystalline lunar spherules: their formation and implications for the origin of meteoritic chondrules. *Meteor. Planet. Sci.* **33**, 13–29.

Takeda, H., Mori, H., Saito, J., Miyamoto, M., 1992. Mineralogical studies of lunar mare meteorites EET 87521 and Y793274. *Proc. Lunar Planet. Sci.* **22**, 355–364.

Taylor, S.R., Bence, A.E., 1975. Evolution of the lunar highland crust. *Proc. Lunar. Sci. Conf. 6th*, 1121–1141.

Taylor, L.A., Shervais, J.W., Hunter, R.H., Shih, C.-Y., Bansal, B.M., Wooden, J., Nyquist, LE., Laul, L.C., 1983. Pre-4.2AE mare-basalt volcanism in the lunar highlands. *Earth Planet. Sci. Lett.* **66**, 33–47.

Taylor, L.A., Patchen, A., Taylor, D.H.S., Chambers, J.G., McKay, D.S., 1996. X-ray digital imaging petrography of lunar mare soils: Modal analysis of minerals and glasses. *Icarus* **124**, 500–512.

Taylor, L.A., Anand, M., Neal, C., Patchen, A., Kramer, G., 2004a. Lunar meteorite PCA 02007: a feldspathic regolith breccia with mixed mare/highland components. *Lunar Planet. Sci.* **XXXV**, CD-ROM #1755 [Abs.].

Taylor, L.A., Patchen, A., Floss, C., Taylor, D., 2004b. An unusual meteorite clast in lunar regolith breccia, PCA 02007. *Meteor. Planet. Sci.* **39**, A105 [Abs.].

Warren, P.H., 2003. The Moon. In: Davis, A.M. (Ed.), *Treatise in Geochemistry*, vol. 1. Elsevier, Amsterdam, pp. 559–599.

Warren, P.H., Kallemeyn, G.W., 1989. Elephant Moraine 87521: the first lunar meteorite composed of predominantly mare material. *Geochim. Cosmochim. Acta* **53**, 3300–3323.

Warren, P.H., Kallemeyn, G.W., 1991. The MacAlpine Hills lunar meteorite and implications of the lunar meteorites collectively for the composition and origin of the Moon. *Geochim. Cosmochim. Acta* **55**, 3123–3138.

Wood, J.A., Dickey, J.S., Marvin, U.B., Powell, B.N., 1970. Lunar anorthosites and a geophysical model of the Moon. *Proc. Lunar Sci. Conf. 1st*, 965–988.

Zeigler, R.A., Korotev, R.L., Jolliff, B.L., 2004. Petrography of lunar meteorite PCA 02007, a new feldspathic regolith breccia. *Lunar Planet. Sci.* **XXXV**, CD-ROM #1978 [Abs.].

Zeigler, R.A., Korotev, R.L., Jolliff, B.L., Haskin, L.A., 2005a. Petrography of lunar meteorite MET 01210, a new basaltic regolith breccia. *Lunar Planet. Sci.* **XXXVI**, CD-ROM #2385 [Abs.].

Zeigler, R.A., Korotev, R.L., Jolliff, B.L., Haskin, L.A., 2005b. Petrography and geochemistry of the LaPaz ice field basaltic lunar meteorite and source-crater pairing with Northwest Africa 032. *Meteor. Planet. Sci.* **40**, 1073–1102.

Zinner, E., Crozaz, G., 1986a. A method for the quantitative measurement of rare earth elements by ion microprobe. *Int. J. Mass Spec. Ion Proc.* **69**, 17–38.

Zinner, E., Crozaz, G., 1986b. Ion probe determination of the abundances of all the rare earth elements in single mineral grains. In: Benninghoven, A., Colton, R.J., Simons, D.S., Werner, H.W. (Eds.), *Secondary Ion Mass Spectrometry, SIMS V*. Springer-Verlag, New York, pp. 444–446.

Zolensky, M.E., 1997. Structural water in the Bench Crater chondrite returned from the Moon. *Meteor. Planet. Sci.* **32**, 15–18.